



THE UNIVERSITY *of* EDINBURGH

Edinburgh Research Explorer

Hydrodynamic interactions of oscillating wave surge converters in an array under random sea state

Citation for published version:

Tay, ZY & Venugopal, V 2017, 'Hydrodynamic interactions of oscillating wave surge converters in an array under random sea state', *Ocean Engineering*, vol. 145, pp. 382-394.
<https://doi.org/10.1016/j.oceaneng.2017.09.012>

Digital Object Identifier (DOI):

[10.1016/j.oceaneng.2017.09.012](https://doi.org/10.1016/j.oceaneng.2017.09.012)

Link:

[Link to publication record in Edinburgh Research Explorer](#)

Document Version:

Peer reviewed version

Published In:

Ocean Engineering

General rights

Copyright for the publications made accessible via the Edinburgh Research Explorer is retained by the author(s) and / or other copyright owners and it is a condition of accessing these publications that users recognise and abide by the legal requirements associated with these rights.

Take down policy

The University of Edinburgh has made every reasonable effort to ensure that Edinburgh Research Explorer content complies with UK legislation. If you believe that the public display of this file breaches copyright please contact openaccess@ed.ac.uk providing details, and we will remove access to the work immediately and investigate your claim.



Hydrodynamic Interactions of Oscillating Wave Surge Converters in an Array under Random Sea State

Zhi Yung Tay^{a*} and Vengatesan Venugopal^b

^a*Engineering Cluster, Singapore Institute of Technology, 10 Dover Drive, Singapore 138683,
Singapore*

^b*Institute for Energy Systems, School of Engineering, the University of Edinburgh,
Edinburgh EH9 3JL, UK*

* Corresponding Author, zhiyung.tay@singaporetech.edu.sg

Abstract

The oscillating wave surge converter (OWSC) type devices (e.g., an Oyster wave energy converter) generate electric power via rotating motion about the bottom of the device. This type of wave energy converters have a wide power absorption bandwidth which enables the electricity generation at a wide range of wave frequencies. The power produced by the OWSCs could be maximised by configuring individual devices within an array. This paper examines the power production performance of multiple OWSCs in an array under regular, uni-directional irregular wave and multi-directional sea using the industry standard hydrodynamic software WAMIT. The performance of the OWSC array is represented as q -factor, which is a quantity defined as the ratio of the average total power produced in an array to the power produced by an individual OWSC. The results show that the OWSCs arranged in an array would produce both constructive and destructive interferences depending on the wave directions and frequencies. Further, the spreading function, the resonance bandwidth and the optimal spacing between the devices are shown to affect the performance of the OWSC

significantly. The results provide an enhanced understanding of the behaviour and performance of the OWSCs when arranged in an array of different configurations.

Keywords: oscillating wave surge converter array; q -factor; hydrodynamic interactions; power performance; genetic algorithm optimisation.

1. Introduction

The Engineering and Physical Science Research Council (EPSRC) in the UK, supports marine energy research through funding grand challenge projects. The TeraWatt [1] and EcoWatt2050 [2] are the two projects funded by the research council, and the work presented in this paper forms part of project deliverables. One of the core objectives of these two project consortiums is provide the industry on the understanding to the limits of energy extraction by marine energy devices when deployed in array, and their impact on the nearshore and coastal environment as well as the marine ecology. The above projects have developed numerical models which will predict the environmental impact, if any, by deployment of wave and tidal energy converters in a very large scale array. The type of wave energy converters (WECs) considered for the present work is the oscillating wave surge converters (OWSC) as these devices possess relatively high capture width ratio of up to 60% [3]. The performance of the OWSC array subjected to different wave conditions is the subject of this paper.

As a means to reduce carbon emission from the burning of fossil fuel to generate energy, the electricity production from renewable energy has increased in popularity in the recent decades [4]. In 2010, the world electricity production from renewable resources totals an amount of 4,160 TWh. This is about 20% of the global electricity production of 21,500 TWh. Out of the total renewable energy production, less than 2% (60TWh) was generated from waves and tidal resources [5]; and this quantity can be considerably increased by deploying large scale array of

wave and tidal energy converters for successful technologies. While some of the individual device concepts are shown to perform well, deploying multiple devices in array would need careful planning for its successful long term operation in extremely complex sea environments. The multi-array arrangement could capture the wave energy effectively if the WECs are designed and arranged in its optimised configuration.

In order to assess the performance of the array, a parameter known as the interaction factor, also known as the q -factor [6], is commonly used to facilitate the discussions. Child and Venugopal [7] have investigated the optimal configuration of point absorber type WEC array using the so called parabolic intersection and genetic algorithm methods by taking the q -factor as the objective function. They have shown that the optimised layout of the wave farms could be used to tune the performance of the WECs. The efficiency of the power absorption of multi-resonant oscillating water column devices has been investigated by Thiruvengatasamy and Neelamani [8] by experimental methods for various device spacings. Sarkar *et al.* [9] considered the wave effects of an oscillating wave surge converter and a heaving point absorber placed adjacent to each other. The findings reported in [7-9] confirmed that the hydrodynamic efficiency of the WECs increases when the array are spaced at their optimum spacing. Borgarino *et al.* [10] investigated the wave interaction effects on the energy absorption in large array of generic wave energy converters and they claimed that the grouping of the WECs into array had a constructive effect when the damping of the power take-off is tuned properly and when the WECs have a large bandwidth.

A comprehensive work on the Oyster type OWSC was carried out in the Queen's University Belfast and University of Dublin [11-12] where they employed a semi-analytical solution to solve for the radiation and scattering problem. They confirmed that high levels of capture factor

can be attained, even though the OWSC is not tuned to resonance with the incident wave field. Renzi *et al.* [13] have investigated the wave-power extraction from a single array of in-line Oyster OWSCs under regular waves by modifying the semi-analytical method; and they observed that the constructive interference is possible for certain period of the incident wave field and claimed that the array with the strongest constructive interaction is accompanied by the largest system efficiency. Renzi *et al.* [13] further reported that the energy extraction of a staggered array of Oyster OWSCs by using the modified semi-analytical and finite-element methods, and claimed that the finite element method (FEM) has advantages over the semi-analytical method due to its flexibility in reproducing virtually any array layouts, for arbitrary angle of incident of the incoming waves, and ensures an excellent reproduction of domains with complex geometries.

For the present work, the boundary element method (BEM) is utilised in assessing the performance of the OWSC array. Similar to the FEM, the BEM also enables the investigation of arbitrary array layouts for any incident wave angle and takes into account the full diffracting and scattering of waves. However, the computational time for the BEM could be greatly reduced when a large wave field is considered as only the boundary integral equation (BIE) of the submerged body wetted surface needs to be solved by employing the free surface Green's function [14]. The utilisation of the BEM is well established in investigating the hydrodynamic interaction of multiple floating bodies as reported in [15-17] and other non-OWSC type of WEC [16, 18-20]. For the first time in this paper, the BEM method is used to investigate the performance of the OWSC type WEC and the industry standard wave interaction analysis software WAMIT [21] has been selected as it has gained widespread recognition in the industry and research organisations i.e. project consortiums and EPSRC expert panels, for its ability to analyse complex structures with a high degree of accuracy and efficiency. Furthermore, the

higher order boundary element method (HOBEM), an option available in WAMIT, is also employed to enhance the computational performance.

The OWSC device considered in the array is similar to that of the Oyster OWSC. As the present study considers a full scale array of OWSCs, there are some difficulties encountered in representing an Oyster type device with its PTO system, as the device information is commercially sensitive and it is not available in the public domain. Hence the results from WAMIT modelling is verified with their counterparts presented by Renzi and Dias [22]. These verified hydrodynamic properties and PTO damping are given here for the benefit of other interested researchers in calibrating or verifying their hydrodynamic models. Together with the hydrodynamic properties, the pitch RAO and q -factor of the array under regular waves are also presented. In addition, we consider the effect of a more realistic sea by modelling the uni-directional irregular wave and multi-directional sea to study the device performance. A new set of results based on 12 OWSCs array arranged in a three-row configuration (known hereafter as the triple-array) is considered and the interaction factors (the q -factor) for the triple-array under regular and irregular waves are presented.

The authors were aware of the recently published papers by Sarkar *et al.* [23-24] and Noad and Porter [25] which also investigated the performance of OWSC arrays. Although there are inevitable similarities between the present paper and the two above mentioned papers, the present paper aims in investigating the hydrodynamic interactions of multiple staggered arrays by taking into consideration the fully diffracted and radiated waves. The array layout investigated here is also based on a more realistic layout following the information given by the Scottish Government Agency – the Marine Alliance for Science and Technology for Scotland (MASTS) [26]. The hydrodynamic effects of the devices in each row towards another

is being studied. As opposed to the semi-analytical method with a thin-rigid plate approximation used in [23] and [25], the present paper takes into account the thickness of the OWSC which should not be neglected due to its significant effect towards the hydrodynamic performance of the device as proven in [27]. The effect of directional spreading in the multi-directional sea is also taken into account in investigating the performance of the array. In addition to that, the influence of the resonance bandwidth towards the performance of the arrays is being investigated and the genetic algorithm optimisation scheme is being introduced to seek for the optimal spacing of the arrays. To the knowledge of the authors, these two areas of investigation on the OWSC type of wave energy device have not yet been published elsewhere in the literature.

The result presented here provide a greater understanding on the behaviour of large-scale array under the influence of a more realistic sea. It also offers a useful insight to the wave energy designers on ways to increase the energy efficiency by properly configuring the devices' spacing and resonance bandwidth. Last but not least, the optimal layout configuration of the array could be designed based on the understanding of the interaction behaviour of devices in the array. It must be noted here that the effect of viscous losses is being compromised in this paper due to the use of the linear potential theory that on the other hand allows the benefit of computational efficiency in running the hydrodynamic analysis of large-scale array in a multi-directional sea.

2. Problem Definition

The triple-array oscillating wave surge converters considered for the hydrodynamic interaction study is shown in Fig. 1. Each OWSC comprises of the flap-type floating body (known

hereafter as the flap) which is hinged at the bottom to a foundation, hence only allowing for the rotational motion about the hinge. The flap PTO system is modelled by a force represented by the damping coefficient B_{pto} to convert the kinetic energy into electricity. The flap has a width a , immersion depth d , thickness t and the hinge is located at a height c from the sea floor. The seabed is considered to be flat with a constant water depth of D . Waves approach the OWSC from an angle θ with a wave frequency ω . The OWSCs are then grouped into a three-row configuration where the first row comprises of five devices, second row four devices and third row three devices, thus a total of 12 OWSCs are placed in the wave farm. Each of the OWSC is separated by a distance s_p as shown in Fig. 1. The global X - Y coordinate system is located at the centre of the OWSC marked as $n = 3$ (see Fig. 1). The vertical coordinate, Z takes zero value at the free and undisturbed water surface. The local coordinate system (x,y,z) is at the hinge of each OWSC. The superscripts in s_p will be used in describing the optimisation process presented in Section 5.5.

The problem at hand is to determine the hydrodynamic interaction of the triple-array under the influence of regular, uni-directional irregular wave and multi-directional sea. Two wave spectra represented by the Pierson-Moskowitz (PM) and the JONSWAP formulations are considered and the wave-structure interaction under these spectra will be presented.

3. Mathematical Formulation

3.1 OWSC under Regular Wave

The OWSC as shown in Fig. 2 is subjected to regular waves with period T and wave height $2A$, where A is the wave amplitude, which pass the structure at a wave angle θ with respect to the X -axis. The motion of the OWSC is assumed to be governed only by the pitch motion Θ , where the other five degree-of-freedom (i.e. surge, sway, heave, roll and yaw) are fixed due

to the hinge boundary condition. The water domain is denoted by Ω whereas the symbol S_F , S_B , S_s and S_∞ denotes the free surface, the seabed, the wetted surface of the OWSC and the artificial boundary condition at infinity, respectively.

3.1.1. Governing Equation for Water Motion

The water is assumed to be an ideal fluid with no viscosity, incompressible and the fluid motion to be irrotational. Based on these assumptions, the fluid motion may be represented by a velocity potential $\Phi(x, y, z, t)$. We consider the water to oscillate in a steady-state harmonic motion with the circular frequency ω . The velocity potential $\Phi(x, y, z, t)$ could be expressed into the following form

$$\Phi(x, y, z, t) = \text{Re}\{\phi(x, y, z)e^{-i\omega t}\} \quad (1)$$

The single frequency velocity potential $\phi(x, y, z)$ must satisfy the Laplace equation [28] and the boundary conditions on the surfaces as shown in Fig. 2. These boundary conditions are given in [21, 28].

The Laplace equation together with the boundary conditions on the surface S are transformed into a BIE by using the 2nd Green's Theorem via a free surface Green's function given in [21] that satisfies the surface boundary condition at the free water surface S_F , the seabed S_B and at the infinity S_∞ . Hence, only the wetted surface of the bodies S_s need to be discretised into panels so that the boundary element method could be used to solve for the diffracted and radiated potential. For details on the Green's function used in solving the BIE, refer to [21].

3.1.2. Governing Equation for OWSC Pitch Motion

The OWSC with a moment of inertia I , PTO damping B_{pto} and restoring moment K is assumed to be a rigid body oscillating with a pitch motion $\Theta(x, y, t)$ at a frequency ω and is subjected to wave forces F . The pitch motion $\Theta(x, y, t)$ could then be written as

$$\Theta(x, y, t) = \mathcal{G}(x, y)e^{-i\omega t} \quad (2)$$

and the corresponding equation of motion is given by

$$-\omega^2 I \mathcal{G} - i\omega B_{pto} \mathcal{G} + K \mathcal{G} = F \quad (3)$$

where, the moment of inertia is given as

$$I = \rho_m V \left(\frac{t^2 + 4d^2}{12} \right) \quad (4)$$

where, ρ_m and V are the mass density and volume of the bodies, respectively. B_{pto} is the optimum PTO damping obtained from [29]

$$B_{pto} = \sqrt{\frac{[K - \omega^2(I - I_a)]^2}{\omega^2} + B_a^2} \quad (5)$$

where, I_a and B_a are the added inertia and radiated damping, respectively. Note that B_{pto} varies with respect to the wave frequency ω , however, the PTO damping is taken as a constant in WAMIT by taking the minimum value of the B_{pto} generated from (5). This value is found from

calibration with known results published in the literature review as will be shown later in Section 4.

F comprises the wave force components which can be derived from the velocity potential $\phi(x, y, z)$ as,

$$F = i\rho\omega \int_S \phi \cdot \mathbf{n} \cdot dS \quad (6)$$

where \mathbf{n} is the normal unit vector to S [21]. As the velocity potential ϕ in Eq. (6) could be further decomposed into the diffracted ϕ_D and radiated ϕ_R part [21, 30], this gives us the exciting moment F_e which is derived from the diffracted potential

$$F_e = i\rho\omega \int_S \phi_D \cdot \mathbf{n} \cdot dS \quad (7)$$

and the added inertia I_a and radiated damping B_a which is derived from the radiated potential

$$(I_a)_{ij} - \frac{i}{\omega} (B_a)_{ij} = \rho \iint_{S_s} \phi_j n_i \cdot dS \quad (8)$$

where ϕ_j is the unit-amplitude radiated potential given in [31]. The indices i and j can take on any values within the ranges of the rigid-body modes (1 to 6) where 1 denotes surge, 2 sway 3 heave, 4 roll, 5 pitch and 6 yaw. For the OWSC, j is taken as 5 which denotes its pitch motion. The equation of motion (3) could then be written as

$$-\omega^2(I + I_a)\vartheta - i\omega(B_{pto} + B_a)\vartheta + K\vartheta = F_e \quad (9)$$

246

247 For N numbers of OWSCs, the equation of motion of body n due to body m is written as

248

$$-\omega^2[I + (I_a)_{nn}]\vartheta_n - i\omega[B_{pto} + (B_a)_{nn}]\vartheta_n + K\vartheta_n - \sum_{\substack{m=1 \\ m \neq n}}^M [\omega^2(I_a)_{mn} + i\omega(B_a)_{mn}]\vartheta_m = (F_e)_n \quad (10)$$

250

251 3.2 OWSC under Uni-Directional Irregular Wave and and Multi-Directional Sea

252 For studying the device performance in random seas, both the Pierson-Moskowitz (PM) and

253 the JONSWAP wave spectra [32] are considered and are expressed by Eqs. (11) and (12),

254 respectively.

255

$$S_{PM}(\omega) = 5\pi^4 \frac{H_s^2}{T_p^4} \cdot \frac{1}{\omega^5} \exp\left[-\frac{20\pi^4}{T_p^4} \cdot \frac{1}{\omega^4}\right] \quad (11)$$

257

$$S_{JONSWAP}(\omega) = \beta_j \cdot S_{PM}(\omega) \cdot \gamma^b \quad (12)$$

259

260 where, g is the gravitational acceleration, ω the wave frequency, ω_p the peak wave frequency,

261 T_p the peak wave period ($2\pi/\omega_p$) and H_s the significant wave height. The peak enhancement

262 factor γ is taken as 3.3 and b depends on the parameter σ given as [32]

263

$$b = \exp\left(-\frac{\omega - \omega_p}{2\sigma^2 \omega_p^2}\right) \quad (13a)$$

$$\sigma = \begin{cases} 0.07 & \text{for } \omega < \omega_p \\ 0.09 & \text{for } \omega > \omega_p \end{cases} \quad (13b)$$

and β_j is given as

$$\beta_j = \frac{0.0624}{0.23 + 0.0336\gamma - 0.185(1.9 + \gamma)^{-1}} (1.094 - 0.01915 \ln \gamma) \quad (14)$$

Sample spectral densities for both PM and JONSWAP spectra for a significant wave height $H_s = 3\text{m}$ and wave peak period $T_p = 10\text{s}$ are presented in Fig. 3.

For the multi-directional sea generation, the uni-directional wave spectrum $S_I(\omega)$ is multiplied by the spreading function $D(\theta)$ as given in Eq. (15).

$$S_I(\omega, \theta) = S_I(\omega) \cdot D(\theta), \quad \text{where } I = \text{PM or JONSWAP} \quad (15)$$

where,

$$D(\theta) = \frac{1}{\sqrt{\pi}} \frac{\Gamma(s+1)}{\Gamma(s+1/2)} \cdot \cos^{2s}(\theta - \bar{\theta}) \quad -\pi/2 < (\theta - \bar{\theta}) < \pi/2, \quad (16)$$

where, $\bar{\theta}$ is the mean wave direction and Γ the gamma function which ensures that

$$\int_{-\pi/2}^{\pi/2} D(\theta) \cdot d\theta = 1 \quad (17)$$

The wave spreading parameter s is taken as 10 which covers a typical of sea conditions according to the results presented in [32]. The directional wave spectrum for the PM and JONSWAP spectra are, respectively, shown in Figs. 4(a) and 4(b) for $H_s = 3\text{m}$, wave peak period $T_p = 10\text{s}$ and mean direction $\bar{\theta} = 0^\circ$.

3.3 Generated Power and Interaction factor

By solving the equation of motion (10), the pitch response amplitude operator (RAO) of the OWSC can be obtained. This then can be used to derive the power generated by the n^{th} OWSC by using the following expression [33]

$$P_n = \frac{1}{2} B_{pto} \omega^2 |RAO|_n^2 \cdot (A/a)^2 \quad (18)$$

The RAO for the pitch motion produced from WAMIT is dimensionless which is defined as

$$RAO = \mathcal{G}(A/a).$$

In order to quantify the interaction between devices, Budal [6] defines the q -factor which is adopted here in Eq. (19) to facilitate the discussion on the performance of the array. For regular waves this is written as,

$$q = \frac{\sum_{n=1}^N P_n}{N \times P_0} \quad (19)$$

where, P_n is the generated power by the n^{th} number of OWSCs and P_0 the generated power of an isolated OWSC. Equation (19) is used as a performance evaluator for the array where a constructive interaction is denoted by a value greater than 1.0 and a destructive interaction when smaller than 1.0.

For uni-directional irregular wave and multi-directional sea, the average power generated over the range of wave frequency considered ω by the n^{th} OWSC is expressed by [33]

$$P_I|_n(\omega) = \int 2P_n(\omega)S_I(\omega, \theta)d\omega \quad (20a)$$

$$P_I|_n(\omega, \theta) = \iint 2P_n(\omega)S_I(\omega, \theta)d\omega d\theta \quad (20b)$$

where, $I = \text{PM or JONSWAP}$. The q -factor for the above cases is then given by

$$q = \frac{\sum_{n=1}^N (P_I)_n}{N \times (P_I)_0} \quad (21)$$

It is noted here that q given in Eqs. (19) and (21) are the average q -factor for the triple array with $N = 12$ devices.

A modified version of the q -factor given, denoted as $q^{Q^{\#}}$ in Eq. (22) has been used to represent the q -factor for only a particular row,

$$q^{Q^h} = \frac{\left(\sum_{m=1}^M P_m \right)_{Q^h}}{M \times P_0} \quad (22)$$

where, M is the total number of OWSCs in the Q^h row.

4. Verification of Numerical Model

The objective of the work is to simulate a realistic wave energy conversion device and its array; hence a WEC which would represent the working principles similar to the Oyster wave energy device [www.aquamarinepower.com] has been chosen for the study. In order to verify the numerical approach, an OWSC width $a = 26$ m, immersion depth $d = 9$ m, thickness $t = 4$ m and water depth $D = 12.5$ m has been considered. These particulars are the same as in [22], except that the thickness t value used in [22] is not known as it is considered trivial in the assumption made in the semi-analytical method derived in [34]. The values of the moment of inertia I and the PTO damping B_{pto} are obtained from Eqs. (4) and (5), respectively. As Oyster device particulars are not in the public domain, several iterations of trial and error are performed to calibrate the restoring moment K and mass M against the results published in [22]. These particulars are summarised in Table 1. In their work, Renzi and Dias [22] made a comparison between the exciting force, added inertia and radiated damping of a single OWSC (denoted as $n = 0$) with that of two OWSCs (denoted as $n = 1$ and 2) arranged in an in-line array. The spacing between the OWSCs in the array is 30m. They also investigated the interaction factor between these two configurations by comparing the q -factor. For the present study, analysis on these two aforementioned configurations (with the same notations of n) is carried out using WAMIT and the results are shown in Fig. 5. For the array with two devices (i.e., $n = 1$ and 2), because of the symmetry in the device arrangement to the wave propagation

direction (i.e. $\theta = 0^\circ$, headsea), no variation in the above hydrodynamic parameters have been noticed between the two devices. The HOBEM is used to obtain these hydrodynamic coefficients with a 5th order Gauss Quadrature used for the outer integration and 4th order for the inner integration in evaluating the BIE. The implementation of the HOBEM would decrease the computational time significantly especially when it involves bodies in array as compared to the lower order method. To ensure convergence, the OWSC mesh size is taken as at least 1/6 of the wave length λ as suggested in [35]. The trend of the exciting pitch moment, added inertia, radiated damping and the q -factor obtained from the present WAMIT model are found to be in very good agreement with those presented in [22] indicated by the thicker lines in Fig. 5. Note that the q -mod value presented in Fig. 5(d) is the modified q -factor by Babarit [36] to assess the performance of individual WEC in the array. Also, it is to be noted here that the hydrodynamic coefficients obtained from the present method do not match exactly with those presented in [22] as shown in Fig. 5 due to the different method used where the present method considers a fully diffracted and radiated waves whereas those in [22] are based on the semi-analytical method. Thus, having verified the present modelling techniques for OWSCs, further study with a 12 device array has been undertaken and the results are given in the next section.

5. Results and Discussions

The spacing s_p considered in the triple-array (Fig. 1a) is $1.73a$ (i.e. 45m as suggested in [26]) The wave frequency ω considered in the analysis ranges from 0.1rad/s to 1.3rad/s with a 0.01 rad/s interval and the wave direction θ from 0 to 90deg with a 1deg interval.

5.1 OWSC Array in Regular Waves

Figure 6 shows the comparison of the pitch response amplitude operator (RAO) between the 12 OWSCs included in the array (i.e. $n = 1$ to 12) with an isolated OWSC (denoted as $n = 0$).

The pitch RAO is plotted against the scatter parameter ka , ranging from 0.5 to 4.5, which corresponds to the wave frequencies ranging from 0.1 to 1.3 rad/s. Four different wave directions, i.e. $\theta = 0^\circ, 30^\circ, 45^\circ$ and 60° have been considered. The results presented in Fig. 6(a) show that under 0° heading (headsea), the OWSCs ($n = 1$ to 5) in the first row, which receives the waves first, produce the highest RAO. This is followed by the second row ($n = 6$ to 9) and the third row of devices ($n = 10$ to 12). In all cases, the highest RAO is found for lower values of ka . The pitch RAO gradually decreases with the increase in wave propagation angle. Also, when the wave heading increases to $30^\circ, 45^\circ$ and 60° , the difference between the pitch RAO between three rows becomes less obvious as there is a smaller difference in the wave energy encountered by each row in the triple-array.

The effects of the wave propagation direction θ and scatter parameter ka on the q^{Q^θ} -factor (see Eq. 22) can also be seen in Fig. 7. In general, the q^{Q^θ} -factors for all the three rows converge close to 1.0 when the scatter parameter is small, i.e. at large wavelength. This is due to the fact that the OWSCs oscillate at the same frequencies without phase difference with the long waves, hence results in minimal wave interaction and diffraction between the devices. In general, for a wide range of ka values, the q^{Q^θ} -factor for the first row appeared to be the highest as compared to those for the second and third rows. It is interesting to note that under headsea condition and when the scatter parameter ka is about 2.50, the q^{Q^θ} -factor for the second and third rows (except $ka > 4.0$) are higher than their counterpart of the first row. This indicates a possibility of increase in wave energy resulting in an increase in pitch motion.

The q -factor (as defined in Eq. 19) summed over all 12 devices is plotted with wave direction θ and scatter parameter ka in Fig. 8(a). This figure shows that the q -factor is the highest when

the wave direction θ is close to 90° and when the scatter parameter ka is the largest. However, by studying the normalised mean power generated $\bar{P} = P/(\rho g V \sqrt{gA})$, where P is the mean power generated by the isolated OWSC (Fig. 8b) and triple-array (Fig. 8c), ρ the mass density of the water, g the gravitational acceleration, V the displaced volume of the OWSC, it can be concluded that the q -factors obtained when the wave direction $\theta > 60^\circ$ are even though higher, their part in power production is insignificant, as the mean power generated corresponding to these q -factors are negligibly small.

By only considering the wave direction $\theta = 0^\circ, 30^\circ, 45^\circ$ and 60° , the q -factor are plotted in Fig. 9. Similar to the observations in Fig. 7, the q -factor converges to 1.0 at small ka values where less scattering from the devices take place. Other observations are: (a) when $\theta = 0^\circ$, destructive interference occurs for ka is less than about 2.60 and changes to constructive interference beyond this limit, (b) when $\theta = 30^\circ$, destructive interference occurs for the whole range of ka considered and (c) when $\theta = 45^\circ$ and 60° , a mixed destructive and constructive interferences occur with different ka values. The gain and fall in q -factor could reach $\pm 20\%$ for the wave approaching from 0° .

5.2 OWSC Array in Uni-Directional Irregular Wave

A typical pitch response spectrum for uni-directional irregular wave corresponding to Pierson-Moskowitz spectrum (same as in Fig. 3) for four different wave directions, i.e. $0^\circ, 30^\circ, 45^\circ$ and 60° are shown in Fig. 10. The response spectrum S_{res} is obtained from the relationship $S_{res} = RAO^2 \times S_{PM}(\omega)$, where S_{PM} is the PM spectrum given in Fig. 3 with a peak period of $T_p = 10\text{s}$ (or $f_p = 0.1\text{ Hz}$). Similar to the pitch RAO plotted in Fig. 6, the magnitudes of the response spectrum for the OWSC array reduces as the wave diverges from the headsea condition. It is

also observed that the peak of the response spectrum slightly shifts its peak response to the left from the peak frequency of the wave spectrum, indicating that the natural frequency of the OWSC is away from the wave frequency and thus resonance will not occur. As OWSC has a wide absorption bandwidth, it could produce power at a wide range of frequencies depending on the wave period T_p of the wave spectrum encountered. Simulations for the JONSWAP spectrum produced a similar trend and hence the results are not included here considering the space limitation.

The q -factors (calculated with Eq. 21) for the array under the PM and JONSWAP spectra are presented in Figs. 11(a) and 11(b), respectively. It is clear that the q -factors for both cases have a similar pattern and order of magnitude for different wave directions and peak periods T_p . The q -factors obtained for four different wave angles, i.e. $\theta = 0^\circ, 30^\circ, 45^\circ$ and 60° are next plotted for both PM and JONSWAP spectra in Fig. 12. The trend in the q -factor for both spectra are almost similar particularly for larger peak periods and the constructive interference between the array only occurs when $\theta = 0^\circ$ and when the wave peak period T_p is approximately smaller than 7s. It is also clear that the q -factor for the array for $\theta = 0^\circ$ decreases with the increase of T_p for the entire T_p range. When the wave period is small, i.e. $T_p < 10$ s, the q -factor for the array under $\theta = 30^\circ, 45^\circ$ and 60° behaves highly irregular with q -factor between 0.65 to 1.0, and this could be due to the strong hydrodynamic interactions (e.g., multiple scattering and radiations) of the OWSCs under short wavelengths. However, it is interesting to note that when T_p is large, i.e. $T_p \geq 10$ s, the behaviour of the q -factors appear to be stable, with a trend that their values increase with the increase of wave angle θ .

5.3 OWSC Array in Multi-Directional Sea

The influence of directional waves on the array performance is presented in this section. For the multi-directional sea generation, both PM and JONSWAP spectra are considered with a spreading parameter s set to 10. Figures 13(a) and (b), respectively, show the q -factor for the array corresponding to the PM and JONSWAP spectra in multi-directional sea and the q factor for the spectra have similar trends. The q -factor is plotted against the mean direction $\bar{\theta}$ and the wave peak period T_p . The constructive and destructive interferences between the devices are found to be strongly linked with the mean wave propagation direction $\bar{\theta}$ and peak wave period T_p , with a maximum constructive interference up to 5%. By focusing on the q -factor along $\bar{\theta} = 0^\circ$, a similar trend as in Fig. 12 can be seen where the constructive interference occur at $T_p = 4\text{s}$ to 7s and then slowly decreases to destructive interference with the increase of T_p . Similarly, at $\bar{\theta}$ between 30° to 60° , the q -factor increases with the increase of $\bar{\theta}$ at large T_p , i.e. $T_p \geq 10\text{s}$. The q -factor in multi-directional sea is observed to be slightly lower than those under regular and irregular waves due to the effect of directional spreading. Hence by comparing the q -factor for the array under regular, irregular and multi-directional sea, the effect of spreading function is significant in influencing the hydrodynamic interaction between the devices in the array. It is emphasize here that the water depth is assumed to be deepwater to the extent that the seabed has no influence towards the random waves generated in this study. However, the effect of depths for shallow water or intermediate water depth could be included in the wave spectra by including a transformation factor to generate a wind-generated sea with fetch limitation such as the TMA spectrum as given in [37].

5.4 Effect of OWSC Resonance Bandwidth

The performance of the OWSC is significantly affected by the resonance bandwidth of the device considered. In order to evaluate the significance of the resonance bandwidth in relation

to the power, two different types of OWSCs have been considered. The first type, hereafter known as OWSC1, has a width $a = 18\text{m}$, immersion depth $d = 9.4\text{m}$, thickness $t = 4\text{m}$ and operates in a water depth of $D = 10.9\text{m}$. While the second type, known here as the OWSC2, has the same dimensions as described in section (4) above. Figure 14 shows the comparison of the normalised mean power generated \bar{P} between OWSC1 and OWSC2, and their corresponding bandwidths are also depicted in the plot. For both OWSC1 and OWSC2, the power generated has been calculated as described in section (3.3). The resonance bandwidth is determined as the frequency range where the power curve cross the horizontal line which is denoted by $P_{\max}/\sqrt{2}$ [29], where P_{\max} is the maximum mean power generated. The plots reveal that OWSC1 has a wider resonance bandwidth as compared to OWSC2; and on the other hand, the latter has a higher mean peak power generated. Notably, the OWSC is a WEC with a wide bandwidth as compared to other types of WECs such as the point absorber and attenuators; hence, the OWSC has a smaller damping coefficient which results in the pitch motion attenuating slowly even when oscillating at high frequency (see Fig. 14). The absorption of wave energy at a wide range of wave frequencies can also be seen in Fig. 14 where the power generated (which is directly related to the pitch motion) does not decay to zero at higher frequencies, with the OWSC1 having a smaller damping coefficient as compared to the OWSC2. Thus, the larger the resonance bandwidth, the greater the capability of the WEC in generating power at the frequency out of the resonance frequency range.

The WAMIT simulations with triple array with one made of OWSC1 and the other of OWSC2 devices have been performed and the corresponding q -factors for the array are plotted against T_p in Fig. 15. Three different wave angles, i.e. $\theta = 0^\circ$, 30° and 45° are considered for this case. As noted in Fig. 12 above, different wave propagation directions have resulted in different q -factor. For headsea condition ($\theta = 0^\circ$), the q -factor for OWSC2 is greater than that of OWSC1

when $T_p \leq 9.5\text{s}$, but a reverse in trend is seen when $T_p > 9.5\text{s}$. At $T_p = 4\text{s}$, the interaction factor for the OWSC2 array increases by about 15% while that of the OWSC1 by about 10%. At $T_p = 16\text{s}$, the interaction factor for OWSC2 decreases by approximately 20% while that of the OWSC1 by 7.5%. The q -factors for both OWSCs appear to be the same at $T_p = 9.5\text{s}$, however with a destructive interference. For other angles, the q -factor for OWSC1 is found to be larger than that for OWSC2 for all wave periods.

5.5 OWSC under Optimal Spacing

The performance of the OWSC array could be optimised through deploying them with appropriate spacing s_p between the devices. The genetic algorithm (GA) optimisation scheme [38] is applied to seek for the optimal spacing between the devices, and for this task only the OWSC2 array has been considered with the objective function to maximise the q -factor. The variables considered in the GA are the spacings s_p^x , s_p^{y1} and s_p^{y2} (refer to Fig. 1 for illustration). The horizontal and vertical spacings between the OWSCs in the array are denoted by s_p^{y1} and s_p^x , respectively, which are kept constant with the maximum allowable spacing of $2a$, where a is the width of OWSC2. s_p^{y2} is the spacing of the OWSC in the second row measured as a distance between its centre of gravity of each device to the centre of s_p^{y1} , with the maximum spacing to be $s_p^{y2} = (s_p^{y1} + a)/2$. The minimum allowable spacing for s_p^x , s_p^{y1} and s_p^{y2} are given, respectively, as $a/5$, a and 0. By a bias distribution of the three spacings of s_p , a good initial population is created. From this initial population, the individuals are created as parents by using the roulette wheel sampling technique [39] for the subsequent crossover and mutation operations in order to create new individual and hence a new generation. The individual with the best fitness value in the current generation is kept for the next generation, which is known

as the elite child. This process will continue until the objective function is met. The crossover and mutation probability are taken as 0.900 and 0.015, respectively. Note that the GA is an in-house code developed by the author in MATLAB.

The headsea direction is considered for the optimisation as the OWSC is most efficient when the waves approach from this direction, i.e. $\theta = 0^\circ$. For demonstration purpose, the q -factors with the possible spacings s_p^{y1} , s_p^x and s_p^{y2} generated from the GA optimisation technique, for regular wave with a period $T = 10$ s, are presented in Figs. 16(a) to (c), respectively. The OWSC in the triple-array deployed at its optimal spacing for $T = 10$ s and $\theta = 0^\circ$ is presented in Fig. 16(d). Figure 16 shows that the q -factor varies with respect to different spacings. It is evident that the values of q takes the largest value when the spacing s_p^{y1} is at its maximum allowable spacing $= 2a$ and the spacing s_p^x is at its minimum allowable spacing $= a$. The optimal spacing for s_p^{y2} has to be close to 0 in order for the q -factor to be maximum. Similarly, the optimal spacings for the OWSC array under different wave period T and wave direction θ could be determined by using the genetic algorithm optimisation technique.

The optimal spacing for s_p^{y1} and s_p^x could be represented by exponential curves as shown in Fig. 17. The data is found to be best fitted by an exponential curve as given in Eq. (23)

$$\bar{s}_p = C_1 e^{C_2(ka)} + C_3 \quad (23)$$

where, ka is the scatter parameter and $\bar{s}_p = s_p/a$, the normalised spacing with respect to the OWSC width a . The coefficients C_1 , C_2 and C_3 are found to be

546

547 $C_1 = -1, C_2 = -1 \text{ and } C_3 = 2 \quad \text{for } s_p^{y1} \quad (24a)$

548

549 $C_1 = 2.5, C_2 = -1 \text{ and } C_3 = 1 \quad \text{for } s_p^x \quad (24b)$

550

551 The comparison of the q -factor for OWSC array with and without spacing optimisation under
552 regular wave and irregular wave are shown in Figs. 18 and 19, respectively. Note that k_{Tp} used
553 in Fig. 19 is the wave number that corresponds to the wave peak period T_p . These figures reveal
554 that the q -factor for the OWSC array could be further enhanced when the OWSCs are spaced
555 at its optimal spacing. By referring to Figs. 18 and 19, under their optimal spacing, it is also
556 possible to create constructive interference which would result in the q -factor > 1.0 for the
557 scatter parameter ka is greater than approximately 1.60. A more comprehensive work on the
558 GA optimisation technique to search for the optimal spacing of OWSC arrays can be found in
559 [40].

560

561 **6. Conclusion**

562 A stochastic analysis to determine the performance of OWSC devices arranged in a triple-array
563 configuration was conducted. The performance of the OWSC array was obtained by using the
564 higher order boundary element method approached in the WAMIT software. The numerical
565 model for the OWSC device in the WAMIT model was successfully calibrated with existing
566 results found in the literature. The verified hydrodynamic properties and PTO damping together
567 with the pitch RAOs and q -factors of the devices were provided for the benefits of researchers
568 working on the same problem.

569

Under the regular wave conditions, it was found that the interaction factors (q -factor) for the oscillating wave energy converter were significantly affected by the exciting force acting on the device, where this in turns depends on the variations in wave frequencies and wave propagation directions. The largest response occurred in the front row of WECs, followed by the middle and last row. However, as the scatter parameter ka is greater than 2.50, it is interesting to note that there was an increase in wave energy in the second and third rows as indicated by the $q^{Q^{\text{th}}}$ -factor. The produced power of the array also became relatively insignificant when the wave propagation direction is greater than $\theta = 60^\circ$. For the dominate wave propagation angle θ at 0° , the constructive interference was found to occur when ka is greater than 2.60, indicated that greater scattering of shorter wave lengths between devices could be beneficial for the performance of the array.

Next, a more realistic sea state based on the uni-directional irregular and multi-directional sea was also taken into account. The performance of the triple-array showed that the interaction factor of the array in a multi-directional sea was slightly lower than their counterparts in a regular and uni-directional sea due the effect of wave spreading. Hence, this spreading function which is often neglected has to be taken into account in the performance analysis of the array. A comparison of the q -factor between those obtained from the Pierson-Moskowitz and JONSWAP spectra revealed that the q -factors do not differ significantly by the choice of the wave spectrum. Under the irregular sea conditions, it is interesting to note that the q -factor for the array under oblique waves behaved in a highly irregular manner when the wave period T_p is smaller than 10s due to the strong scattering and radiations of waves. In contrast, the behaviour of the q -factors appeared to be stable, with their values increased with the increase of θ when T_p is greater than 10s.

In addition, the effect of resonance bandwidth has on the performance of the array was also being investigated. By comparing two OWSCs with different bandwidths under the headsea condition, it was found that the OWSC's ability to generate power corresponds to its bandwidth where the OWSC with a larger bandwidth (i.e. OWSC1) was able to generate greater power when T_p is large (i.e. $T_p > 9.5s$) and conversely, the WEC with a narrow bandwidth (i.e. OWSC2) was able to produce greater power at small T_p (i.e. $T_p \leq 9.5s$). However, the q -factor for OWSC1 was found to be greater than that for OWSC2 for all wave periods under oblique waves.

Lastly, a novel optimisation method based on the genetic algorithm scheme was successfully performed to seek for the optimal spacing of the array with the objective function to maximise the q -factor. The q -factors (for both the regular and uni-directional irregular wave) of the OWSC array under its optimal spacing were found to increase substantially as compared to the initial spacing of 45m as proposed in [26]. Constructive interference was observed when the scattered parameter ka is greater than 1.60. The optimal spacings found from the GA scheme could be approximately represented by exponential curves. These results could be used by wave energy device designers in the design of the array layout during the preliminary design stage.

It is worth bearing in mind that the results presented here were bound by the assumptions of potential wave theory where the fluid viscosity and rotational flow that may exist in real sea conditions were neglected. However, the use of potential theory allowed the investigation of large-scale array under multi-directional sea in a computationally efficient way. In the absence of any real site measurements with WEC array to verify the methods presented here, care must be exercised in applying these results.

7. Acknowledgement

The authors are grateful for the financial support of the UK Engineering and Physical Sciences Research Council (EPSRC) through the EcoWatt2050 research consortium (EPSRC Reference No.: EP/K012851/1).

8. References

- [1] *TeraWatt: Large Scale Interactive Coupled 3D Modelling for Wave and Tidal Energy Resource and Environmental Impact* [cited 2015 5th March 2015]; [Online] Available: <http://gow.epsrc.ac.uk/NGBOViewGrant.aspx?GrantRef=EP/J010170/1>.
- [2] *EcoWatt2050*. [cited 2015 5th March 2015]; [Online] Available: <http://gow.epsrc.ac.uk/NGBOViewGrant.aspx?GrantRef=EP/K012851/1>.
- [3] Babarit, A and Hals, J. On the maximum and actual capture width ratio of wave energy converters. in *Proceedings of the 10th European Wave Energy Conference*. 2011. Southampton, UK.
- [4] International Energy Agency. *2014 Key World Energy Statistic*. Paris, France, 2014.
- [5] World Energy Council. *World Energy Resources 2013 Survey*. England, UK, 2013.
- [6] Budal, K, "Theory for absorption of wave power by a system of interacting bodies", *Journal of Ship Research*, vol.21(4), 1977.
- [7] Child, BFM and Venugopal, V, "Optimal configurations of wave energy device arrays", *Ocean Engineering*, vol.37(16), pp. 1402-1417, 2010.
- [8] Thiruvankatasamy, K and Neelamani, S, "On the efficiency of wave energy caissons in array", *Applied Ocean Research*, vol.19(1), pp. 61-72, 1997.
- [9] Sarkar, D, Renzi, E, and Dias, F, "Interactions between an oscillating wave surge converter and a heaving wave energy converter", *Journal of Ocean and Wind Energy*, vol.1(3), pp. 135-142, 2014.
- [10] Borgarino, B, Babarit, A, and Ferrant, P, "Impact of wave interactions effects on energy absorption in large arrays of wave energy converters", *Ocean Engineering*, vol.41, pp. 79-88, 2012.
- [11] Renzi, E, Doherty, K, Henry, A, and Dias, F, "How does Oyster work? The simple interpretation of Oyster mathematics", *European Journal of Mechanics-B/Fluids*, vol.47, pp. 124-131, 2014.
- [12] Whittaker, T and Folley, M, "Nearshore oscillating wave surge converters and the development of Oyster", *Philosophical Transactions of the Royal Society of London A: Mathematical, Physical and Engineering Sciences*, vol.370(1959), pp. 345-364, 2012.
- [13] Renzi, E, Abdolali, A, Bellotti, G, and Dias, F, "Wave-power absorption from a finite array of oscillating wave surge converters", *Renewable Energy*, vol.63, pp. 55-68, 2014.
- [14] Newman, JN, "Algorithms for the free-surface Green function", *Journal of Engineering Mathematics*, vol.19(1), pp. 57-67, 1985.
- [15] Williams, AN and Abul-Azm, AG, "Hydrodynamic interactions in floating cylinder arrays—II. Wave radiation", *Ocean Engineering*, vol.16(3), pp. 217-263, 1989.
- [16] Wolgamot, HA, Taylor, PH, and Eatock Taylor, R, "The interaction factor and directionality in wave energy arrays", *Ocean Engineering*, vol.47, pp. 65-73, 2012.
- [17] Tay, ZY, Wang, CM, and Utsunomiya, T, "Hydroelastic responses and interactions of floating fuel storage modules placed side-by-side with floating breakwaters", *Marine Structures*, vol.22(3), pp. 633-658, 2009.

- [18] Delauré, YMC and Lewis, A, "3D hydrodynamic modelling of fixed oscillating water column wave power plant by a boundary element methods", *Ocean engineering*, vol.30(3), pp. 309-330, 2003.
- [19] Vantorre, M, Banasiak, R, and Verhoeven, R, "Modelling of hydraulic performance and wave energy extraction by a point absorber in heave", *Applied Ocean Research*, vol.26(1), pp. 61-72, 2004.
- [20] De Backer, G, *Hydrodynamic Design Optimization of Wave Energy Converters Consisting of Heaving Point Absorbers*, 2009, Ghent University: Belgium.
- [21] Wamit Inc, *Wamit User Manual*, 2011, Version 7.0: USA.
- [22] Renzi, E and Dias, F, Wave-power extraction from a finite array of oscillating wave surge converters, *International Workshop on Water Waves and Floating Bodies*, 2013, France.
- [23] Sarkar, D, Renzi, E, and Dias, F. Wave farm modelling of oscillating wave surge converters. in *Proceedings of the Royal Society of London A: Mathematical, Physical and Engineering Sciences*. 2014. The Royal Society.
- [24] Sarkar, D, Contal, E, Vayatis, N, and Dias, F, "Prediction and optimization of wave energy converter arrays using a machine learning approach", *Renewable Energy*, vol.97, pp. 504-517, 2016.
- [25] Noad, I and Porter, R, "Optimisation of arrays of flap-type oscillating wave surge converters", *Applied Ocean Research*, vol.50, pp. 237-253, 2015.
- [26] O'Hara Murray, R. *Pentland Firth and Orkney Waters Round 1 Array Layouts*. Marine Alliance for Science and Technology for Scotland (MASTS), UK, July 2014.
- [27] Renzi, E and Dias, F, "Hydrodynamics of the oscillating wave surge converter in the open ocean", *European Journal of Mechanics-B/Fluids*, vol.41, pp. 1-10, 2013.
- [28] Faltinsen, OM. *Sea Loads on Ships and Offshore Structures*. Vol. 1, Cambridge University Press, UK, 1993.
- [29] Falnes, J. *Ocean Waves and Oscillating Systems*. Cambridge University Press, UK, 2002.
- [30] Wang, CM and Tay, ZY, *Hydroelastic analysis and response of pontoon-type very large floating structures*, in *Fluid Structure Interaction II*. 2010, Springer. p. 103-130.
- [31] Newman, JN and Lee, C-H, "Boundary-element methods in offshore structure analysis", *Journal of Offshore Mechanics and Arctic Engineering*, vol.124(2), pp. 81-89, 2002.
- [32] Goda, Y. *Random Seas and Design of Maritime Structures*. World Scientific, Singapore, 2010.
- [33] Cruz, J, Sykes, R, Siddorn, P, and Taylor, RE, "Estimating the loads and energy yield of arrays of wave energy converters under realistic seas", *IET Renewable Power Generation*, vol.4(6), pp. 488-497, 2010.
- [34] Renzi, E and Dias, F, "Relations for a periodic array of flap-type wave energy converters", *Applied Ocean Research*, vol.39, pp. 31-39, 2013.
- [35] Jafaryeganeh, H, Rodrigues, JM, and Guedes Soares, C, "Influence of mesh refinement on the motions predicted by a panel code", *Maritime Technology and Engineering*, ed. Guedes Soares, C, CRC Press, London. pp, 1029-1038, 2014.
- [36] Babarit, A, "Impact of long separating distances on the energy production of two interacting wave energy converters", *Ocean Engineering*, vol.37(8), pp. 718-729, 2010.
- [37] Massel, SR. *Hydrodynamics of coastal zones*. Vol. 48, Elsevier, 1989.
- [38] Davis, L. *Handbook of Genetic Algorithms*. Vol. 115, Van Nostrand Reinhold, New York, USA, 1991.
- [39] Goldberg, DE and Deb, K, "A comparative analysis of selection schemes used in genetic algorithms", *Foundations of Genetic Algorithms*, vol.1, pp. 69-93, 1991.
- [40] Tay, ZY and Venugopal, V, "Optimization of Spacing for Oscillating Wave Surge Converter Arrays Using Genetic Algorithm", *Journal of Waterway, Port, Coastal, and Ocean Engineering*, vol.143(2), pp. 04016019, 2016.

Table 1: Properties of Oyster2 OWSC model

Properties	Value	Unit
Length a	26	m
Immersion Depth d	9	m
Thickness t	4	m
Water Depth D	12.5	m
Restoring Moment K	12.81×10^6	$\text{kg.m}^2.\text{s}^{-2}$
Mass Moment of Inertia about Centre of Gravity I	9.1455×10^6	kg.m^2
PTO Damping B_{pto}	16×10^6	$\text{kg.m}^2.\text{s}^{-1}$

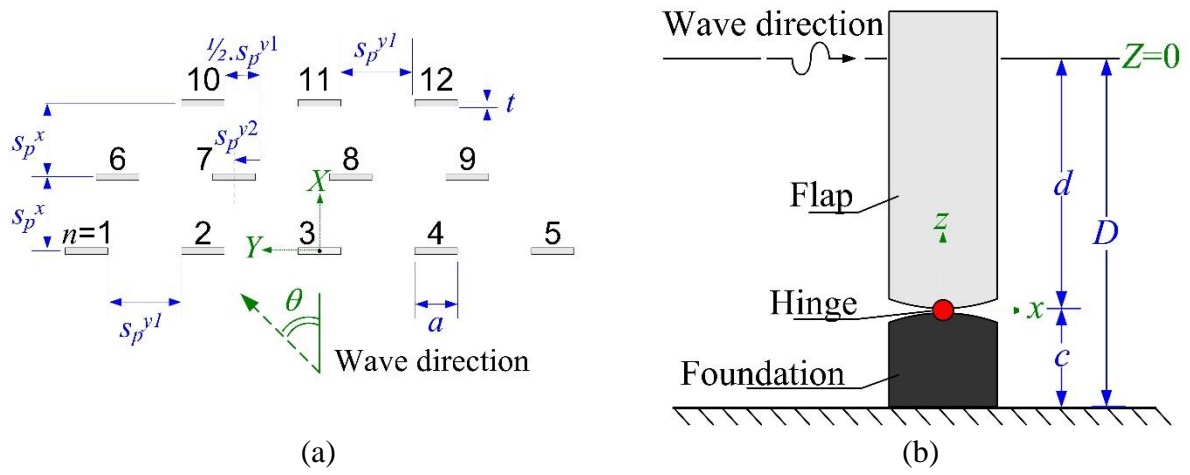


Figure 1 –Plots showing (a) Triple-array configuration of 12 OWSCs in plan view (b) Dimensions for each OWSC.

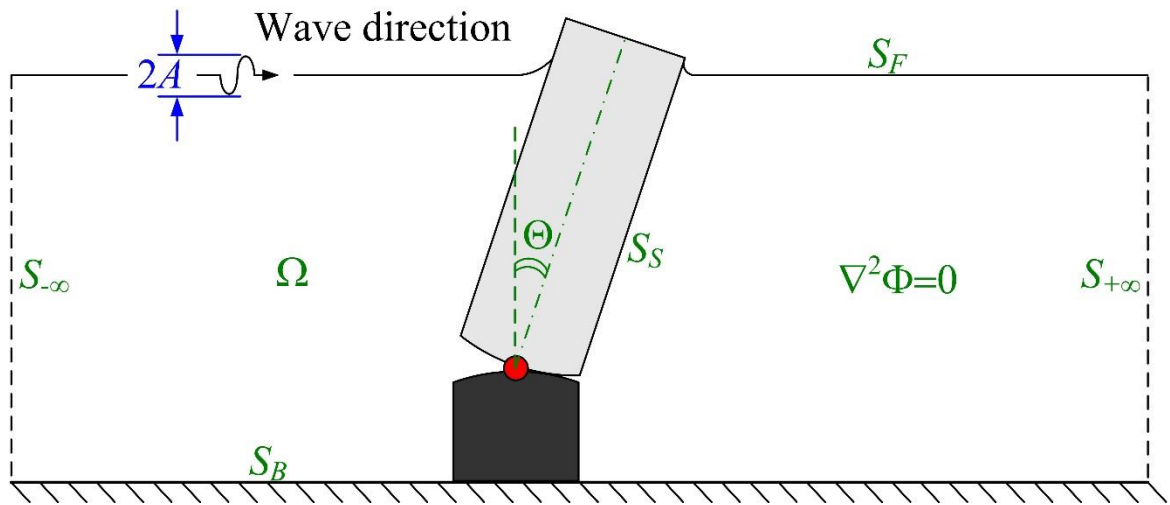


Figure 2 – Schematic diagram depicting mathematical domain of OWSC

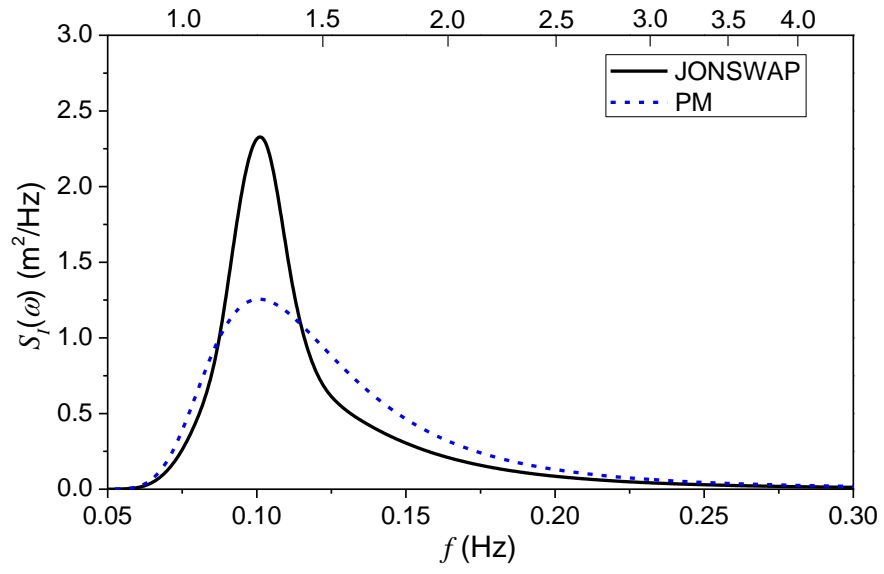


Figure 3 – Comparison of PM and JONSWAP wave spectra. $H_s = 3\text{m}$ and $T_p = 10\text{s}$.

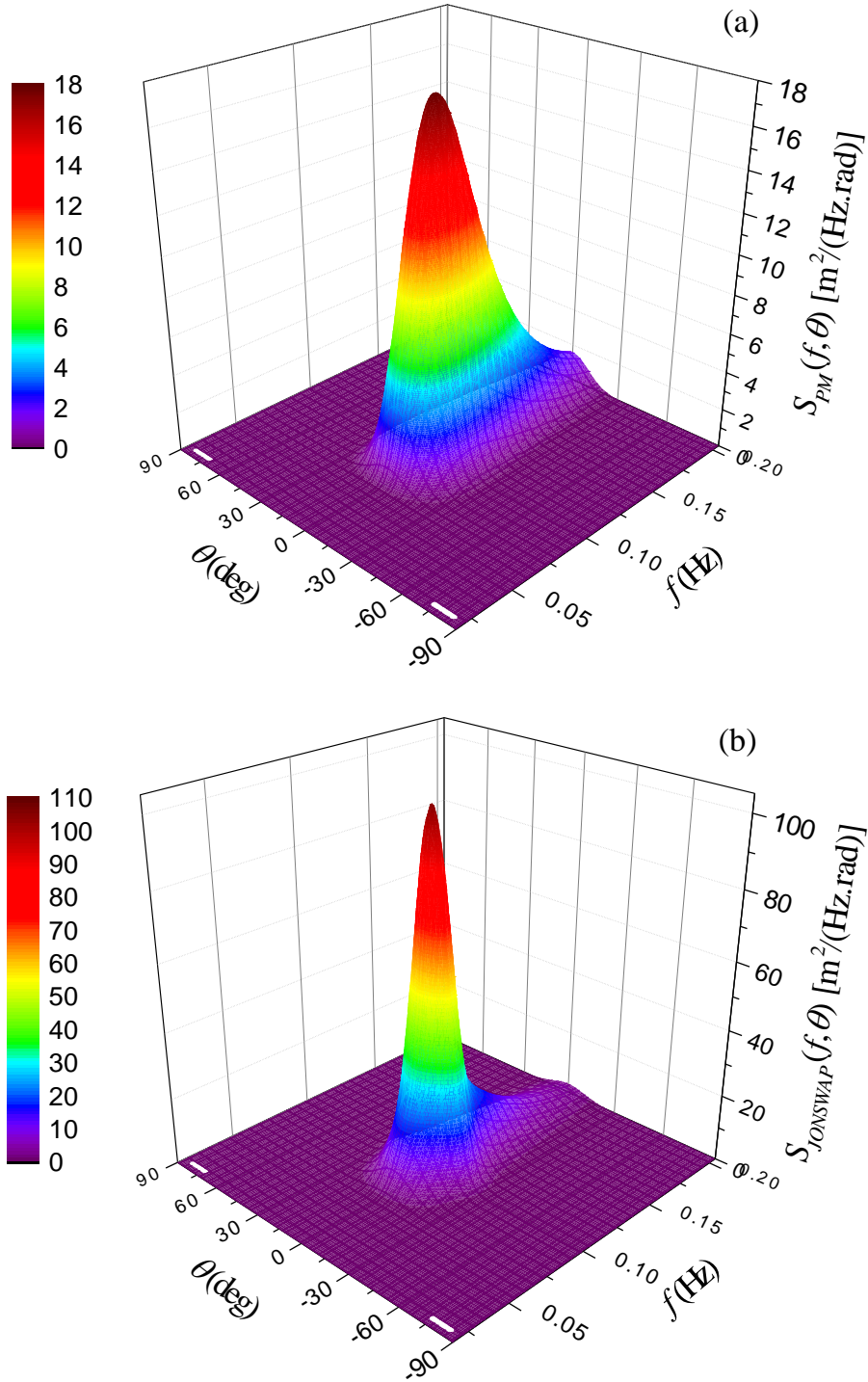


Figure 4 – Multi-directional wave spectrum for (a) PM spectrum (b) JONSWAP spectrum.
 $H_s = 3\text{m}$, $T_p = 10\text{s}$ and $\bar{\theta} = 0^\circ$.

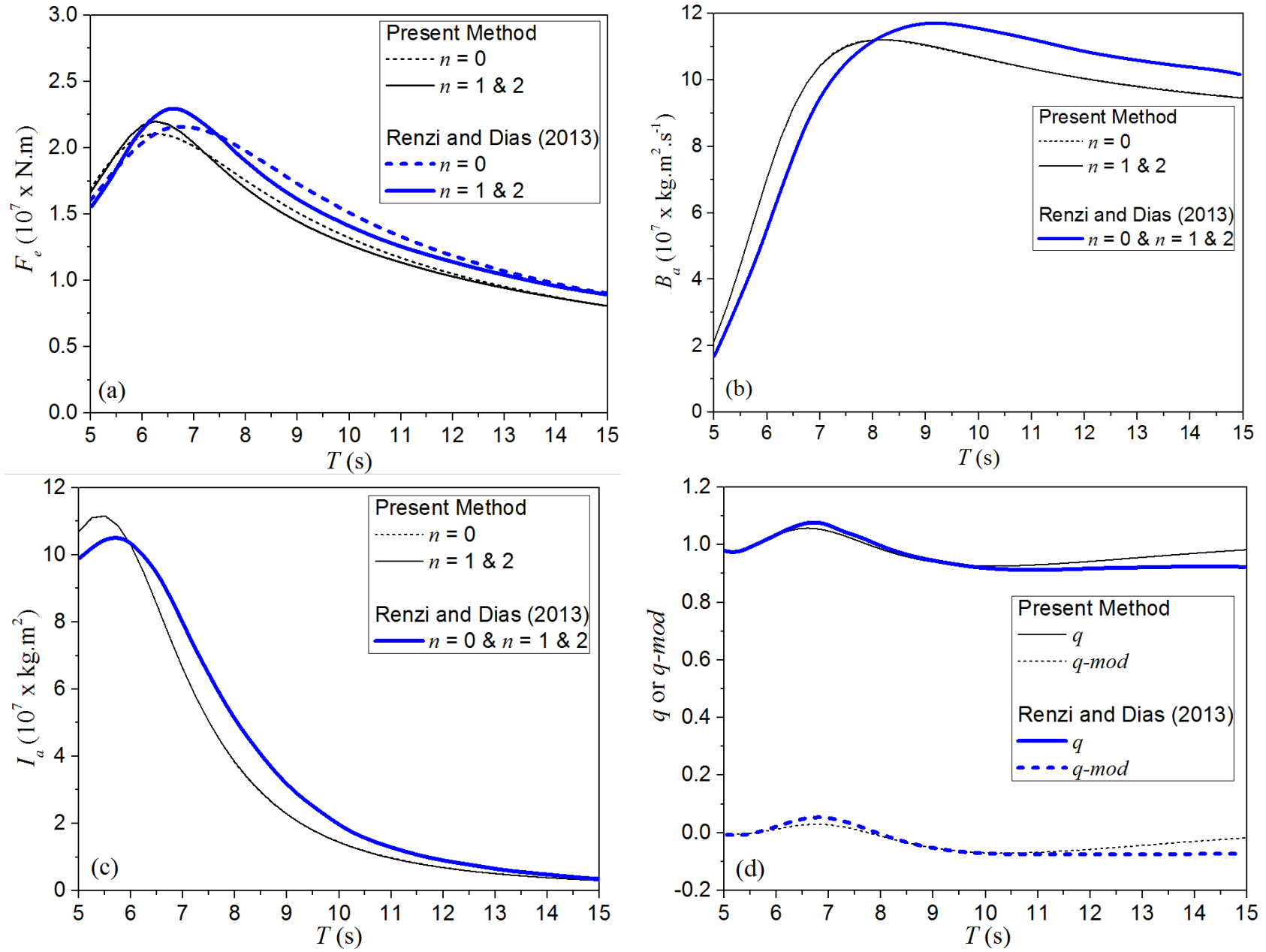


Figure 5 – Hydrodynamic coefficients for Oyster2 OWSC. Water depth $D = 12.5\text{m}$, wave direction $\theta = 0^\circ$. Width $a = 26\text{m}$, thickness $t = 4\text{m}$ and immersion depth $d = 9\text{m}$.

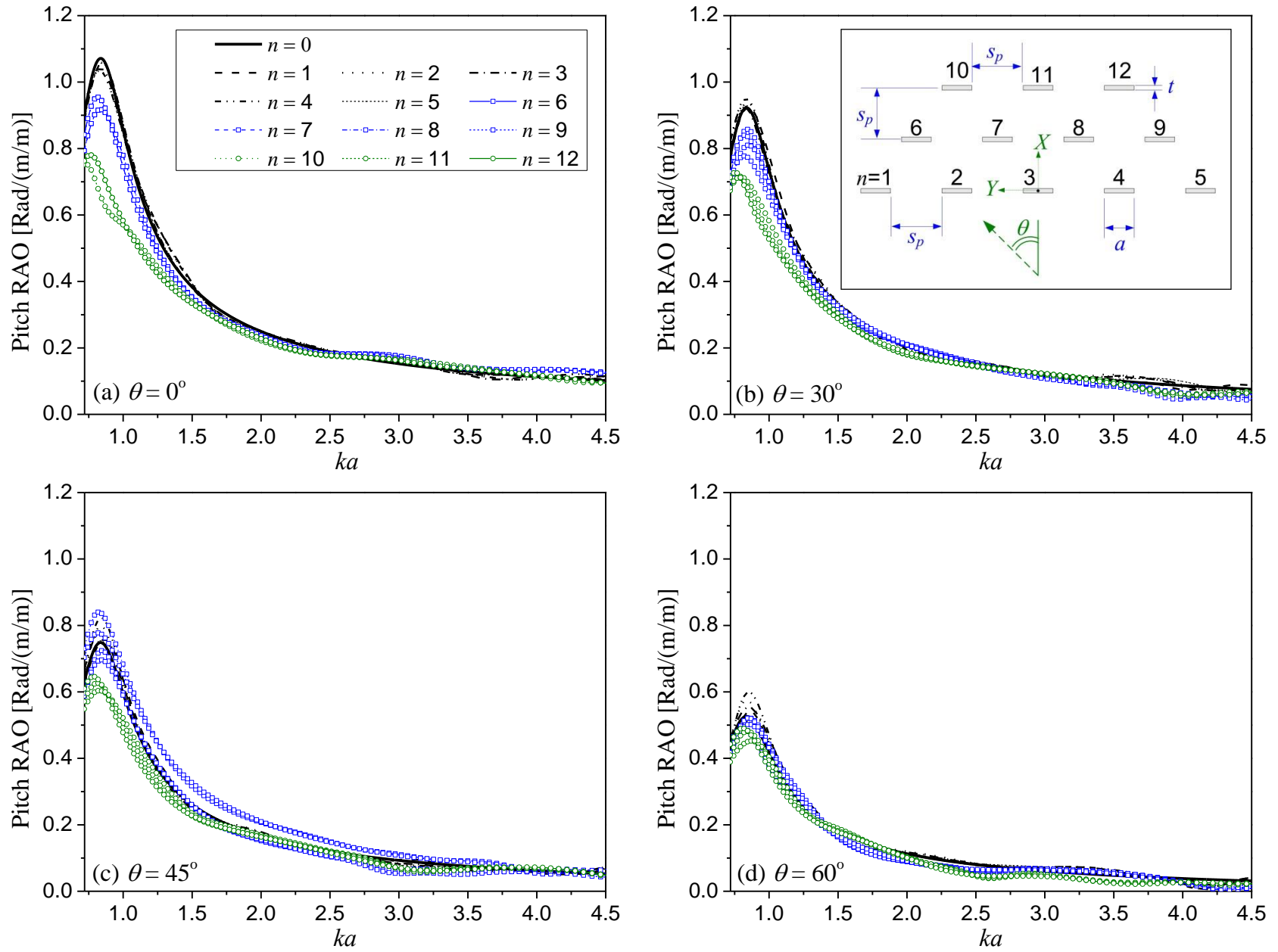


Figure 6 – Comparison of pitch RAO for triple-array OWSC ($n = 1$ to 12) with single OWSC ($n = 0$) under regular wave. (a) $\theta = 0^\circ$ (headsea) (b) $\theta = 30^\circ$ (c) $\theta = 45^\circ$ (d) $\theta = 60^\circ$. Water depth $D = 12.5\text{m}$. Width $a = 26\text{m}$, thickness $t = 4\text{m}$ and immersion depth $d = 9\text{m}$. Spacing $s_p = 45\text{m}$.

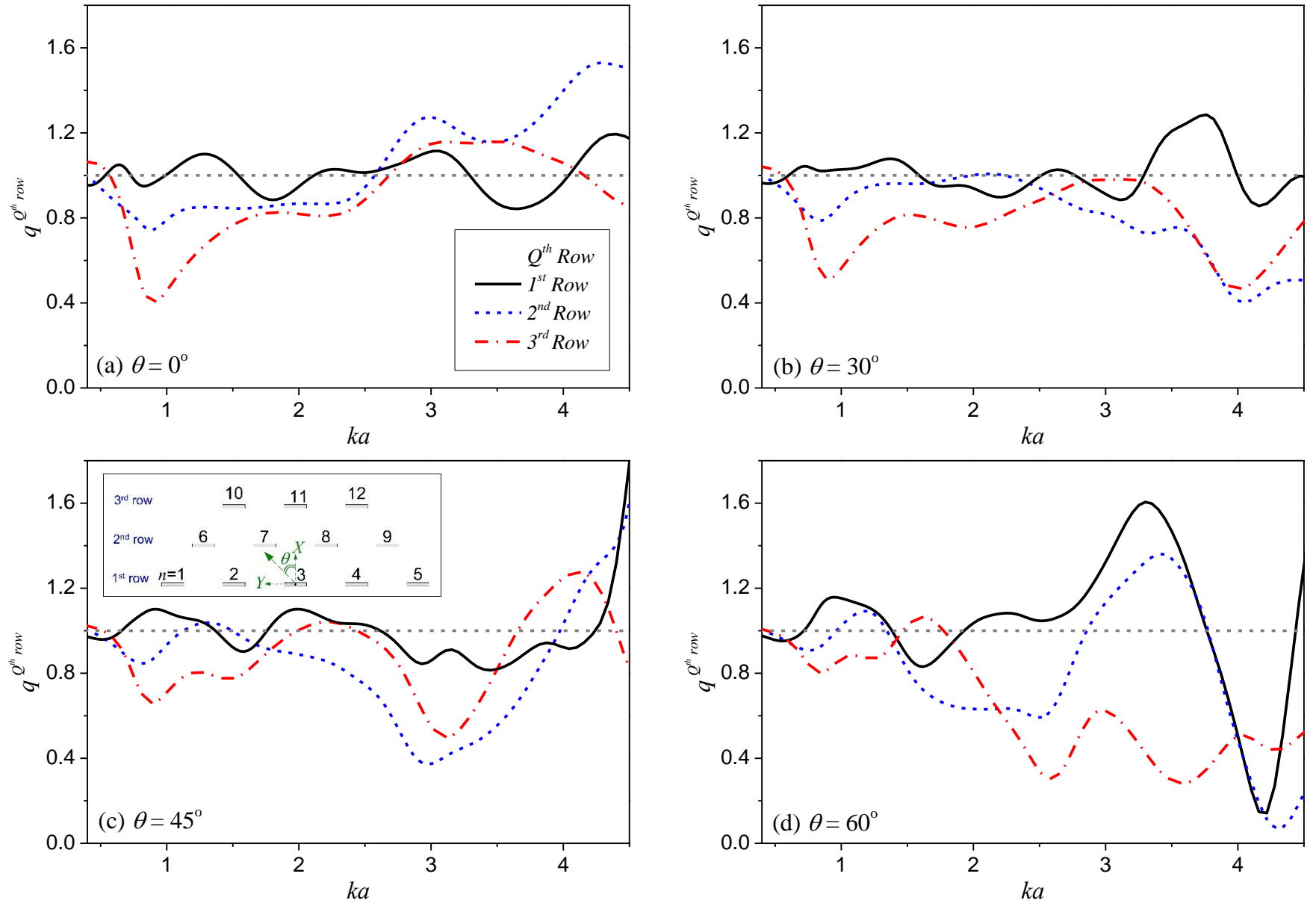


Figure 7 – $q^{Q^{th} row}$ for triple-array under regular wave. (a) $\theta = 0^\circ$ (headsea) (b) $\theta = 30^\circ$ (c) $\theta = 45^\circ$ (d) $\theta = 60^\circ$. Water depth $D = 12.5\text{m}$. Width $a = 26\text{m}$, thickness $t = 4\text{m}$ and immersion depth $d = 9\text{m}$. Spacing $s_p = 45\text{m}$.

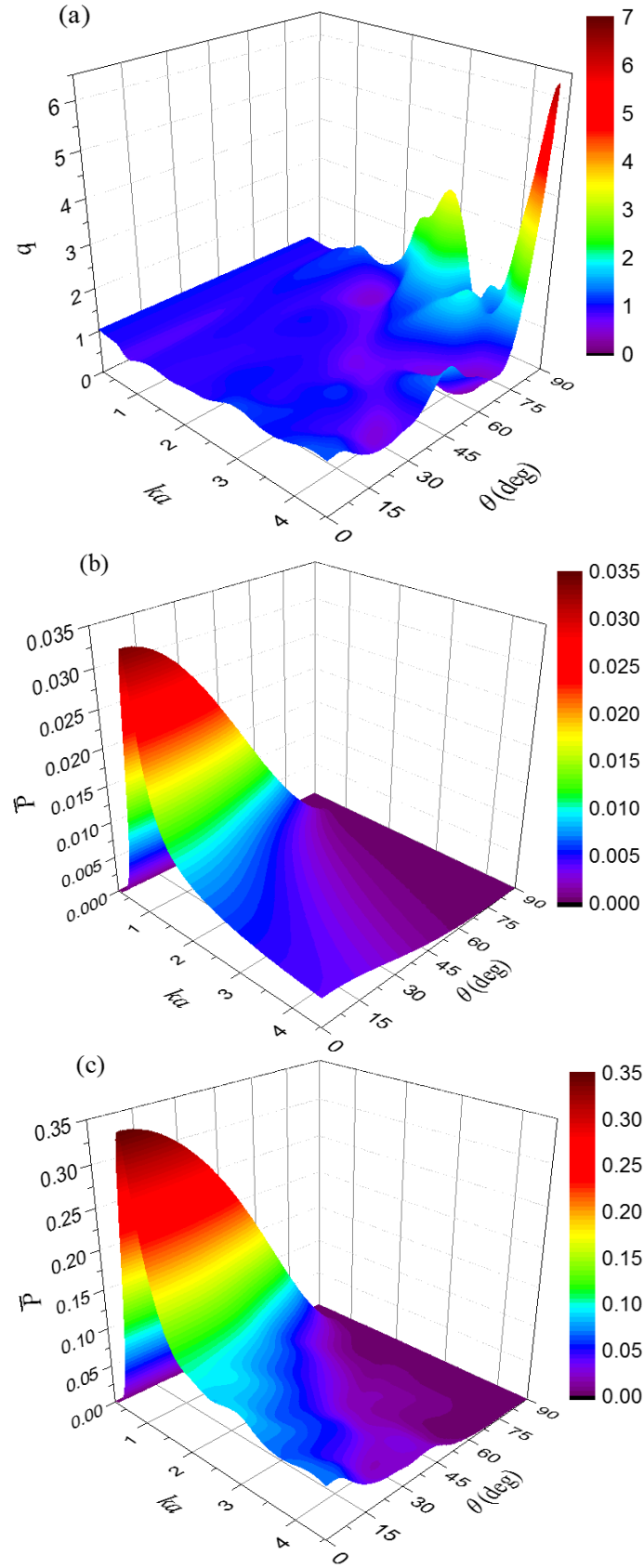


Figure 8 – Plots showing (a) q -factor for triple-array OWSC (b) Normalised mean power generated for single isolated OWSC (i.e. $n = 0$) (c) Normalised total mean power generated for triple-array OWSC (i.e. $n = 1$ to 12), under regular waves.

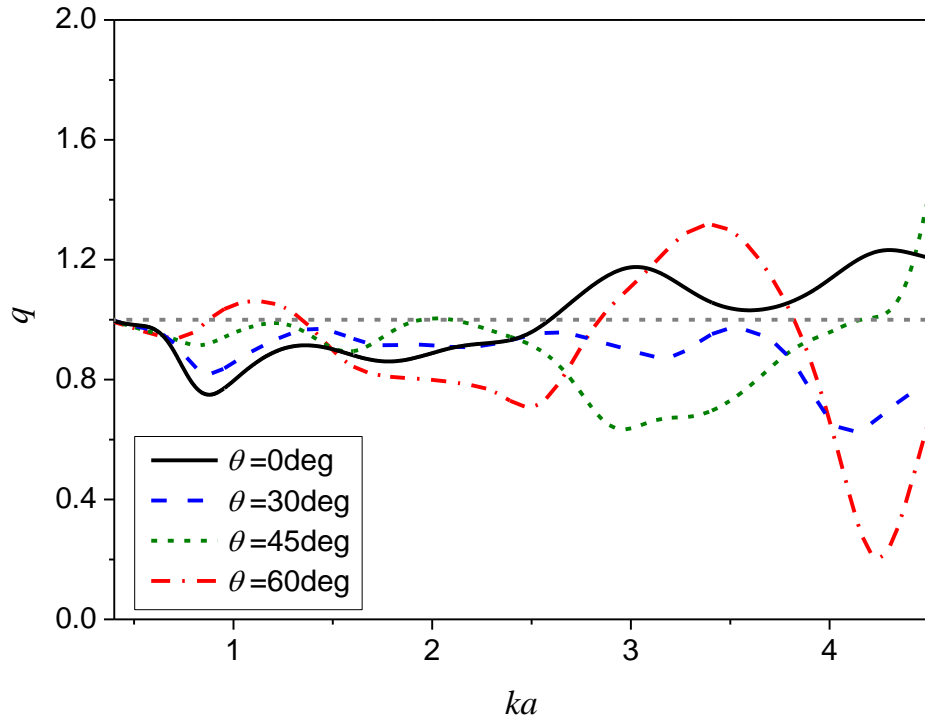


Figure 9 – Comparison of q -factor for triple-array for different wave directions θ under regular wave. Water depth $D = 12.5\text{m}$. Width $a = 26\text{m}$, thickness $t = 4\text{m}$ and immersion depth $d = 9\text{m}$. Spacing $s_p = 45\text{m}$.

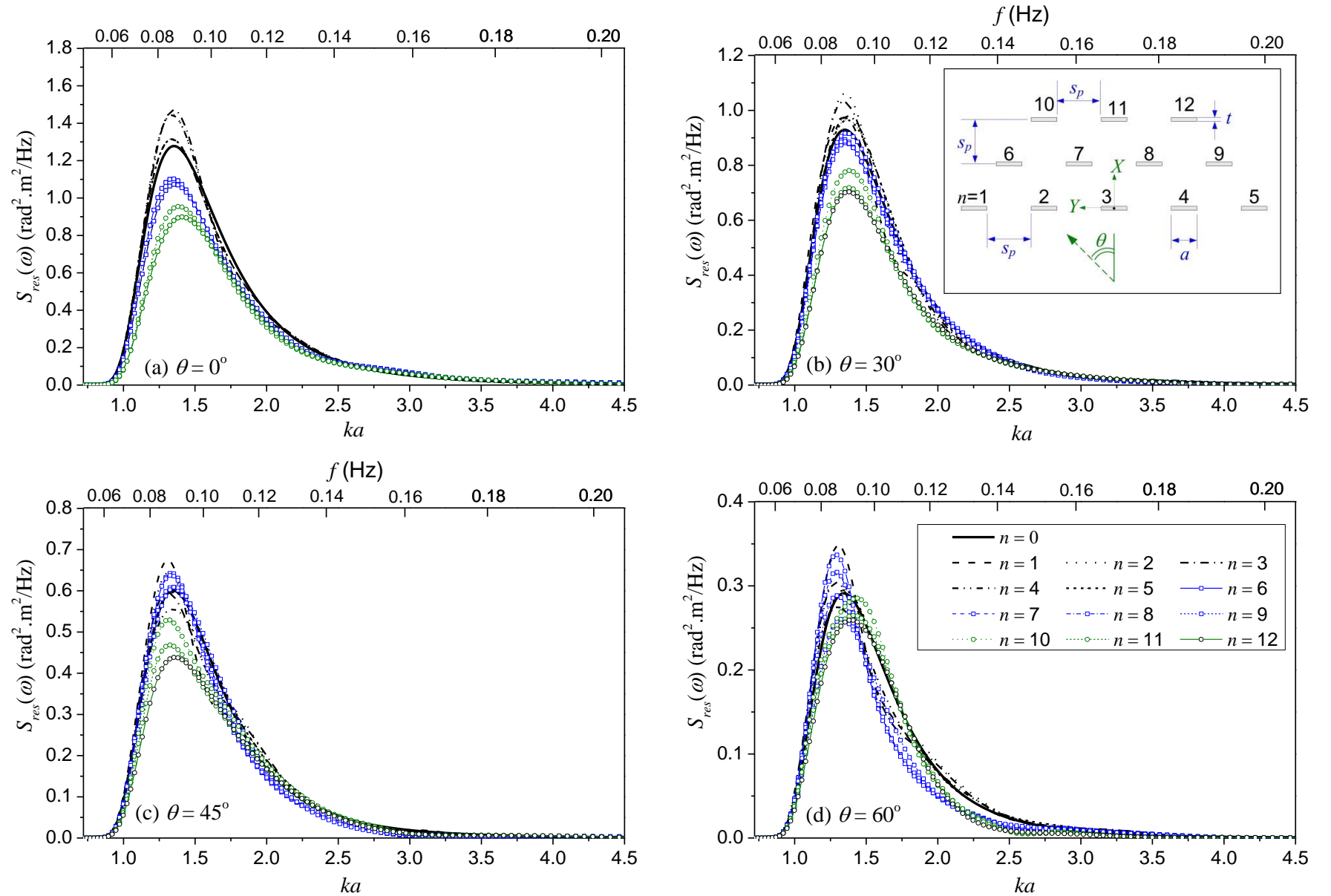


Figure 10 – Comparison of pitch response spectrum S_{res} for triple-array OWSC with single OWSC under uni-directional irregular wave (PM spectrum). Wave heading (a) $\theta = 0^\circ$ (headsea) (b) $\theta = 30^\circ$ (c) $\theta = 45^\circ$ (d) $\theta = 60^\circ$. Water depth $D = 12.5$ m. Width $a = 26$ m, thickness $t = 4$ m and immersion depth $d = 9$ m. Spacing $s_p = 45$ m. $H_s = 3$ m and $T_p = 10$ s.

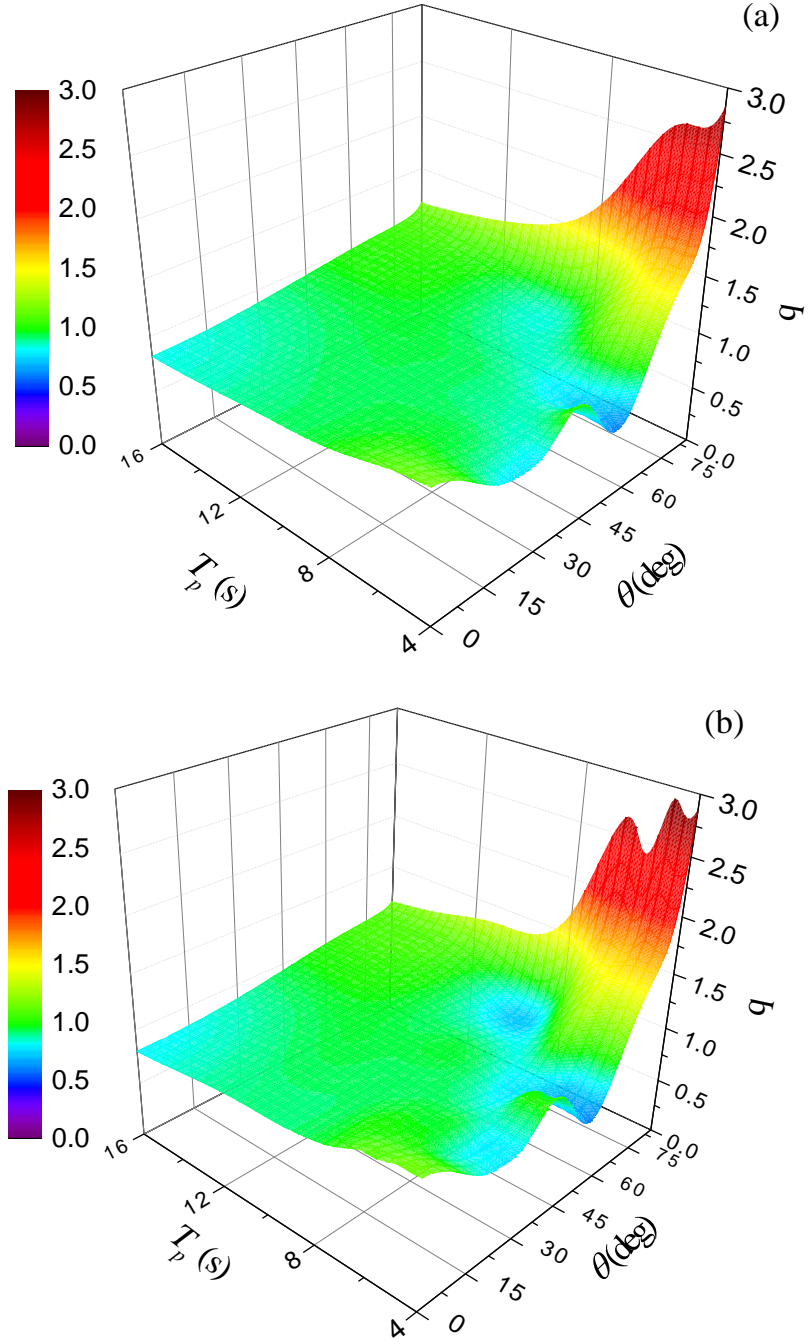


Figure 11 – q -factor for triple-array of OWSC under uni-directional irregular wave (a) PM spectrum (b) JONSWAP spectrum. $H_s = 3$ m.

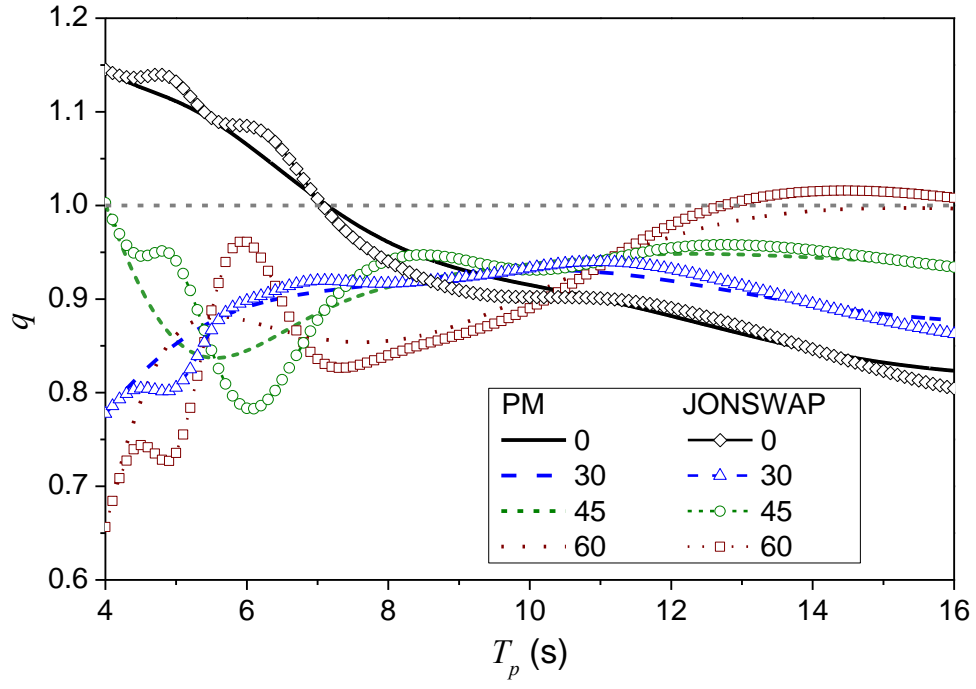


Figure 12 – Comparison of q -factor under different wave directions θ for OWSC ($n=3$) under uni-directional irregular wave (PM and JONSWAP spectra). $H_s = 3\text{m}$.

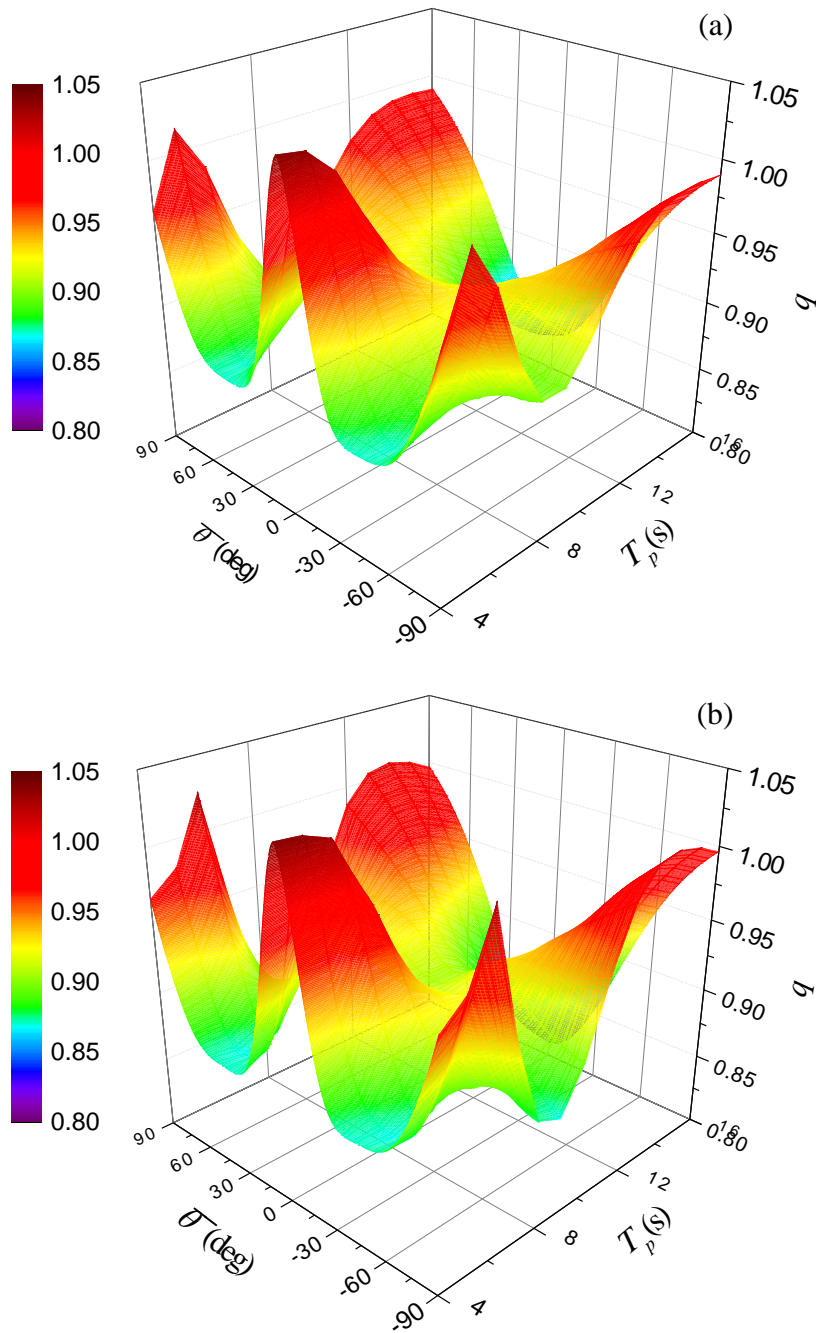


Figure 13 – q -factor for triple OWSC under multi-directional sea with (a) PM spectrum (b) JONSWAP spectrum. $H_s = 3\text{m}$.

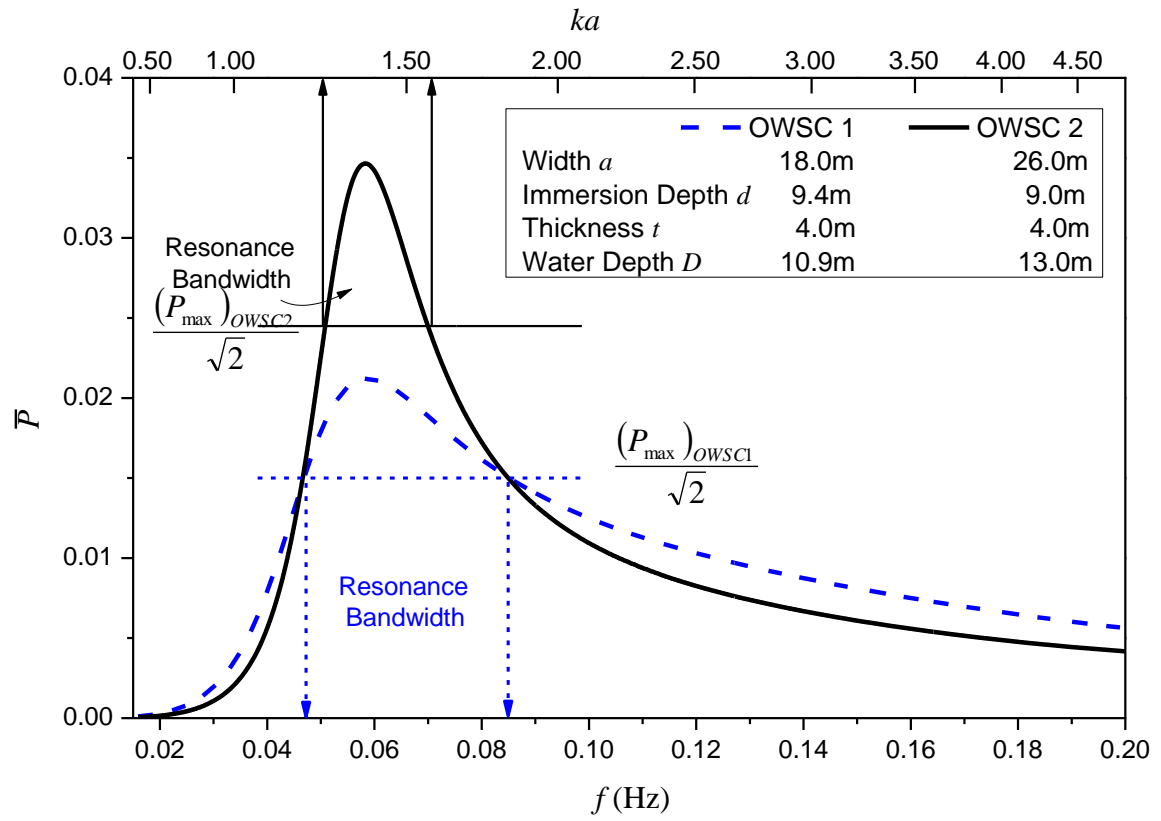


Figure 14 – Comparison of normalised mean power generated \bar{P} for single OWSC1 and OWSC2

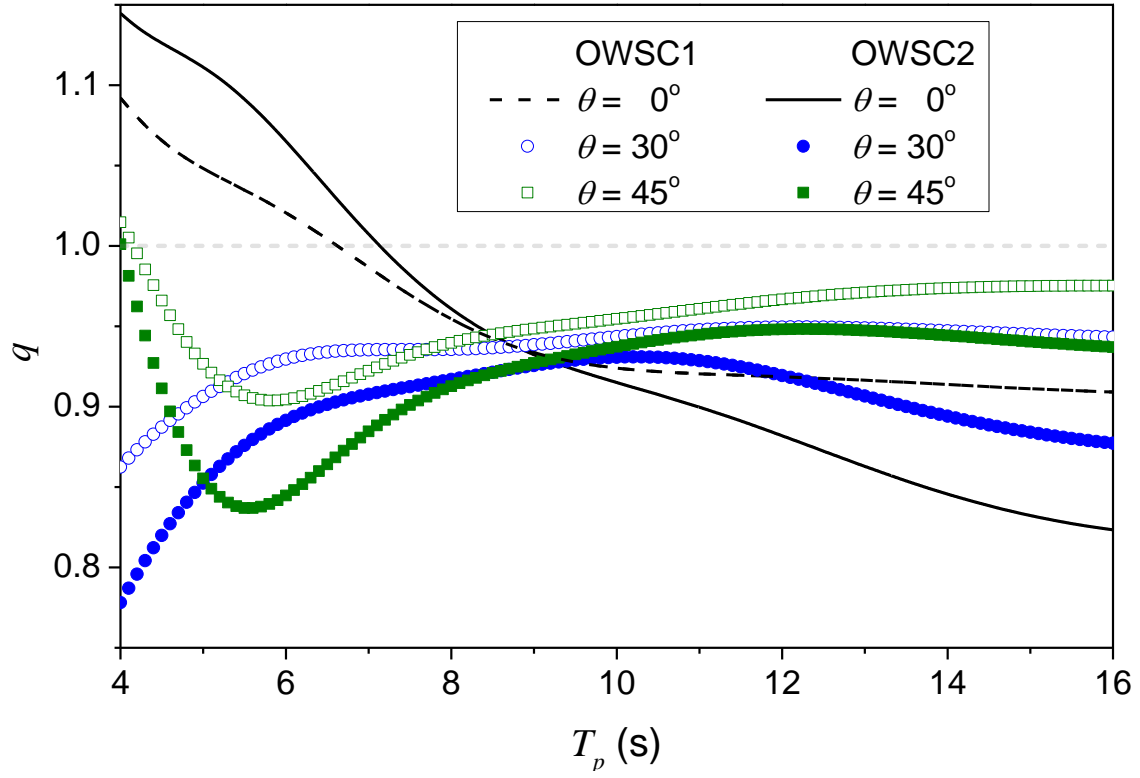


Figure 15 – Effect of resonance bandwidth towards q -factor of triple-array under uni-directional irregular wave (PM spectrum). $H_s = 3\text{m}$.

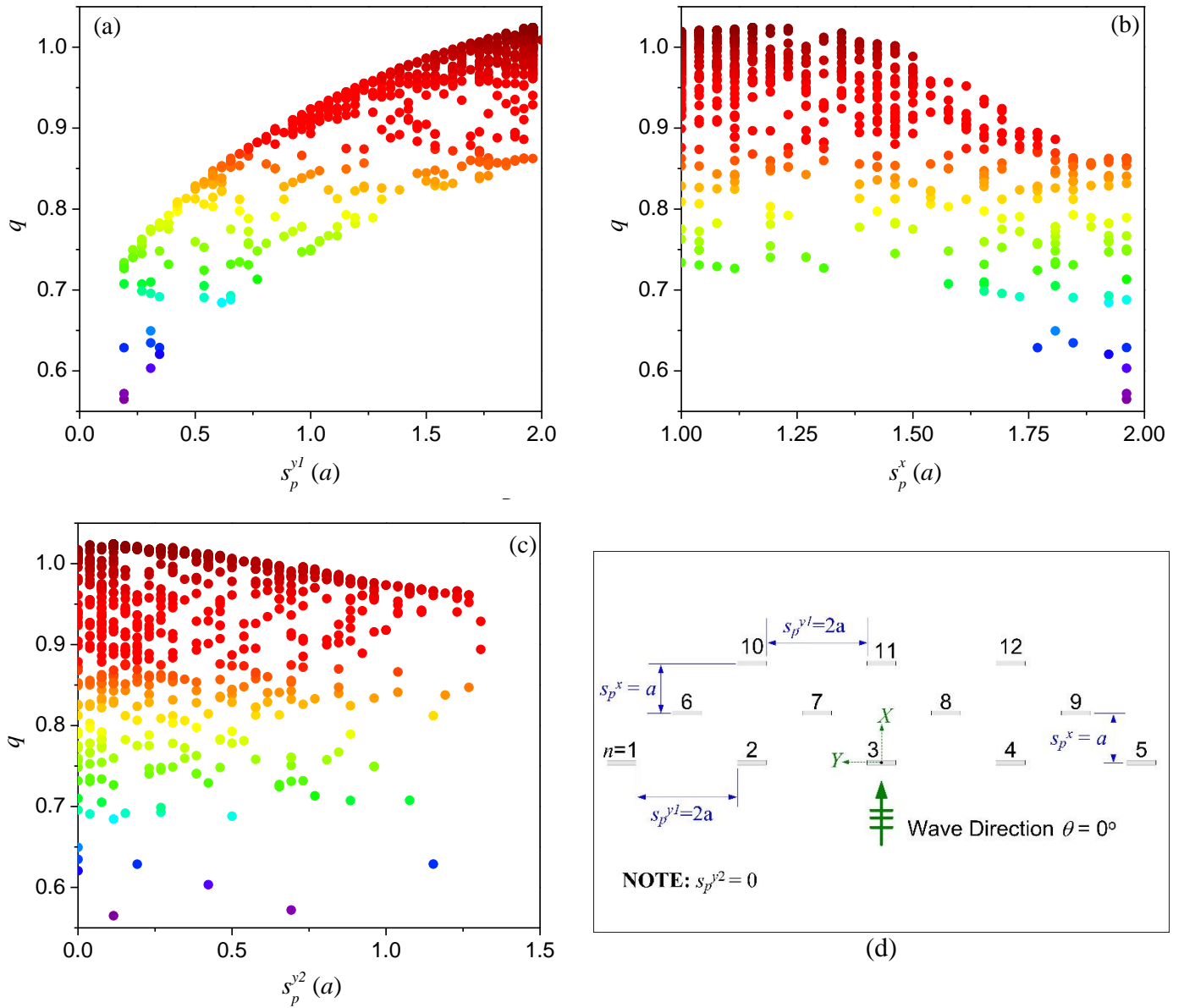


Figure 16 – Example of q -factor for triple-array with respect to (a) spacing s_p^{yl} (b) spacing s_p^x (c) spacing s_p^{y2} (d) triple-array layout under optimal spacing. Wave period $T = 10s$, regular wave amplitude $A = 1m$, wave direction $\theta = 0^\circ$.

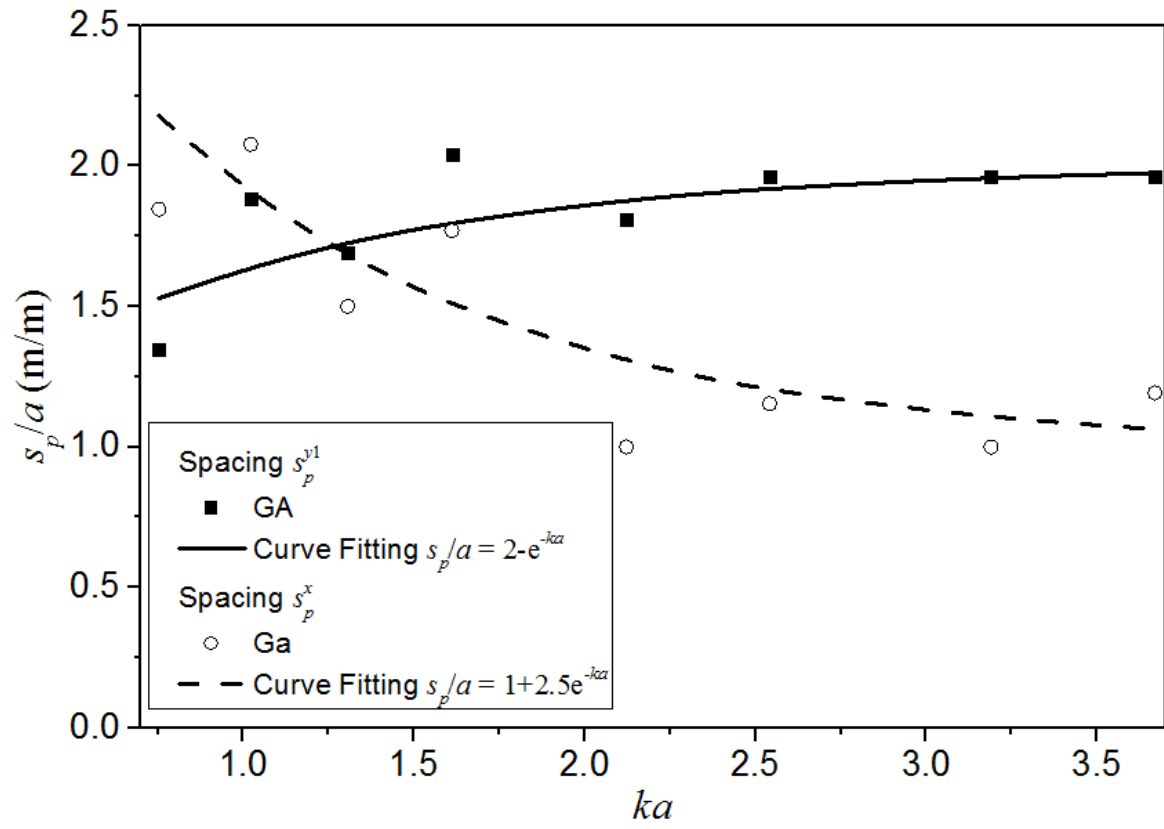


Figure 17 – Optimal spacing for OWSC array represented by exponential curve fitting method

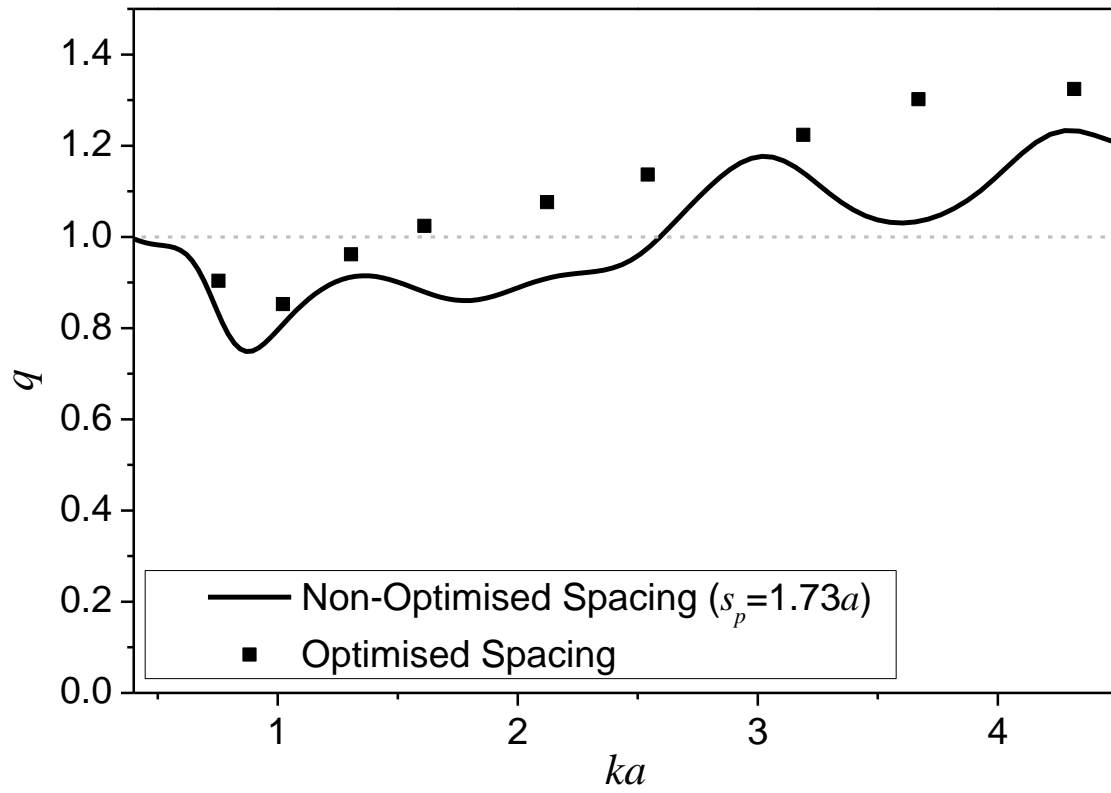


Figure 18 – Comparison of q -factor for OWSC array with and without optimised spacing under regular wave

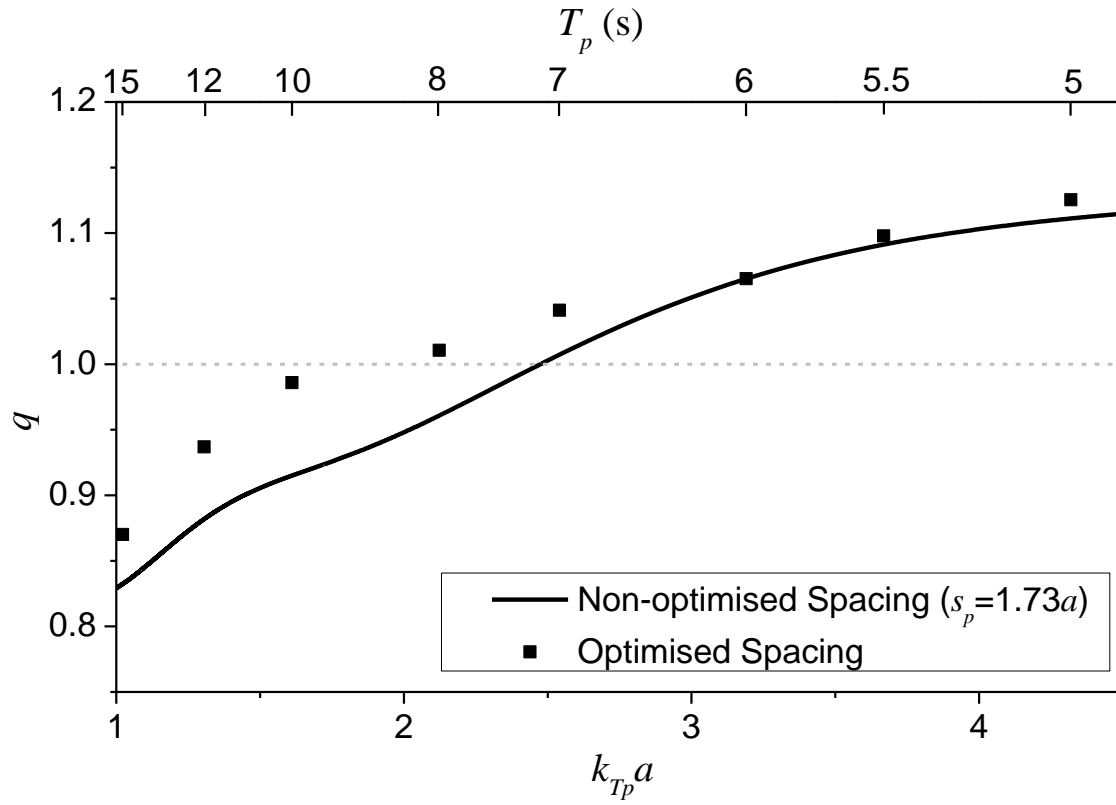


Figure 19 – Comparison of q -factor for OWSC array with and without optimised spacing under PM uni-directional irregular wave. $H_s = 3\text{m}$.